Chronically elevated FGF23 drives sustained renal ERK signaling and inflammatory transcriptional programs mitigated by cFGF23 gene therapy

Adrian Salas-Bastos[1#], Claire Bardet[2#], Klaudia Kopper[1,3], Louisa Jauze[4,5], Fanny Collaud[4,5], Amandine Francois[2,4,5], Matthias B. Moor[6], Gaozhi Chen[7,8], Moosa Mohammadi[7,8], Christian Stockmann[1], Lukas Sommer[1], Johannes Loffing[1,3], Giuseppe Ronzitti[4,5*], Ganesh Pathare[1,3,9*§]

[1]Institute of Anatomy, University of Zurich, Zurich, Switzerland; [2]Université de Paris, Institut des maladies musculo-squelettiques, Laboratory Orofacial Pathologies, Imaging and Biotherapies URP2496 and FHU-DDS-Net, Dental School, and Plateforme d'Imagerie du Vivant (PIV), Montrouge, France; [3]Swiss National Centre of Competence in Research "Kidney Control of Homeostasis", Switzerland; [4]Genethon, 91000 Evry, France; [5]Université Paris-Saclay, Univ Evry, Inserm, Genethon, Integrare research unit UMR_S951, 91000 Evry, France; [6]Department of Nephrology and Hypertension, Inselspital University Hospital, Bern, Switzerland; [7]Oujiang Laboratory (Zhejiang Lab for Regenerative Medicine, Vision, and Brain Health), School of Pharmaceutical Sciences, Wenzhou Medical University, Wenzhou, China; [8]Institute of Cell Growth Factor, Oujiang Laboratory (Zhejiang Lab for Regenerative Medicine, Vision, and Brain Health), Wenzhou, China; [9]Bone-Kidney Axis and Regeneration Laboratory, Department of Infectious Diseases and Public Health, Jockey Club College of Veterinary Medicine and Life Sciences, City University of Hong Kong, Hong Kong SAR

[#] and * contributed equally

[§]**Corresponding author**:
Prof. Ganesh Pathare, BVSc, PhD
Bone-Kidney Axis and Regneration Laboratory
Department of Infectious Diseases and Public Health
Jockey Club College of Veterinary Medicine and Life Sciences
City University of Hong Kong, Hong Kong SAR
Email: gpathare@cityu.edu.hk

Keywords: FGF23, Klotho, X-linked hypophosphatemia (XLH), ERK1/2, inflammatory transcriptome

Competing Interests

L.J. and G.R. are inventors in a patent concerning the treatment of XLH (WO/2020/212626). All other authors declare no conflict of interest.

ABSTRACT

Fibroblast growth factor 23 (FGF23) levels are highly elevated in patients with chronic kidney disease (CKD); however, whether it serves merely as a biomarker or actively contributes to kidney inflammation remains unclear. Full-length FGF23 is cleaved into C-terminal FGF23 (cFGF23), which acts as a natural antagonist of FGF23 by inhibiting its binding to the FGF receptor (FGFR) and the co-receptor Klotho. Here, we show that chronically elevated FGF23 levels in a mouse model Hyp-Duk cause sustained-ERK signaling and an inflammatory and immune responses in the kidney. cFGF23, delivered via adeno-associated virus (AAV) gene therapy, successfully mitigated renal sustained-ERK signaling and inflammatory and immune responses in Hyp-Duk mice. On the other hand, acute physiological FGF23 levels *in vitro* elicited transient-ERK signaling with the expression of canonical early-ERK targets (*EGR1, JUNB, FOSB*). Consistent with *in vivo* findings, prolonged pathological FGF23 treatment *in-vitro* revealed sustained-ERK signaling with upregulation of late-ERK targets (*ETV4/5, SPRED1/2, SPRY2/4*) and unique inflammatory and immune gene signatures. These effects were significantly mitigated by FGFR and ERK inhibitors, as well as by recombinant cFGF23 treatment. In summary, chronically high levels of FGF23 induce kidney inflammation through the FGFR-Klotho complex and sustained-ERK activation, which are successfully mitigated by cFGF23 gene therapy.

TRANSLATIONAL STATEMENT:

Chronically elevated circulating levels of Fibroblast Growth Factor 23 (FGF23) are strongly associated with inflammation and adverse outcomes in chronic kidney disease, but the underlying mechanisms remain poorly understood. Our study identifies sustained activation of the ERK signaling pathway as a key mechanism by which chronic FGF23 elevation induces inflammatory transcriptional programs in the kidney. Importantly, gene therapy using the C-terminal fragment of FGF23 (cFGF23) mitigates these effects, highlighting a potential therapeutic strategy to counteract the excessive FGF23 signaling.

INTRODUCTION

The phosphaturic hormone fibroblast growth factor 23 (FGF23) is primarily produced by osteoblasts and osteocytes[1–3]. FGF23 mediates its phosphaturic effects by inducing asymmetric dimerization of its cognate FGF receptors (FGFR) in the kidneys in a Klotho and heparan sulfate (HS) dual coreceptor fashion[2,4–6]. The 1:2:1:1 FGF23-FGFR-Klotho-HS signaling complex rapidly triggers ERK signaling thus inducing expression of immediate early genes such as *Egr1, Fos* and *Jun,* necessary for regulating mineral metabolism[6–8]. Klotho is a single pass transmembrane protein and is primarily expressed in the kidneys as mice with a kidney-specific Klotho ablation have a similar phenotype as global Klotho knockout mice[9,10]. Klotho is also expressed in in the brain, parathyroid glands, and gonads, albeit in lower levels compared to the kidney[11]. Extracellular shedding results in soluble form of Klotho (sKlotho) that is found in blood, urine, and cerebrospinal fluid[10,12]. sKlotho in supraphysiologic levels can mimic some of the effects of transmembrane Klotho[6,13]. FGF23's bioactivity is principally regulated by a proteolytic cleavage, resulting in inactive larger N-terminal (nFGF23) and C-terminal fragments (cFGF23). Intact (iFGF23 or simply FGF23), nFGF23 and cFGF23 coexist in the circulation[14,15].The isolated cFGF23 peptide inhibits FGF23-Klotho binding thereby suppressing FGF23-mediated regulation of mineral metabolism[16,17].

FGF23 levels are massively elevated in chronic kidney disease (CKD) patients and have been associated with inflammation, cardiovascular disease, morbidity and mortality[18–22]. The fact that chronic administration of cFGF23 alleviated renal and cardiovascular pathobiology in a rodent model of CKD lends credence to the notion that the association between high FGF23 and adverse events is more than a mere association but in fact signifies causality[23]. Whether elevated FGF23 causes kidney inflammation in CKD is not clear[24]. Inflammatory cytokines such as IL-6 and TNF-α are often elevated in CKD patients and may upregulate FGF23 expression in bone, as well as in immune cells and tissues that do not normally express FGF23[18,25–27]. Conversely, elevated FGF23 has been shown to induce inflammation in hepatocytes and immune cells, which do not express Klotho[26,28–30]. The Klotho-independent actions of FGF23 contradict the functional and structural data that proposes the essential role of Klotho in FGF23 function[5,6,13].

FGF23 is elevated in numerous human genetic diseases of hypophosphatemia, including X-linked hypophosphatemia (XLH), which is caused by inactivating mutations in the *PHEX* gene[31,32]. The clinical symptoms of XLH are growth retardation, leg bowing, rickets, osteomalacia, bone pain, and dental illness. Many of these symptoms are phenocopied in various murine models of XLH, whether arising from a spontaneous mutation such as the *Hyp-Duk* mouse or generated by inactivating the *Phex* gene[17,31,33]. To date, no inflammatory lesions have been reported in the kidneys or heart of XLH patients and mouse models who have lifelong elevated FGF23 levels[33–36]. However, recently, one study found that XLH patients have elevated circulatory inflammatory markers, suggesting a possible link between chronic FGF23 elevation and inflammation in XLH[37].

141 Physiological regulators like dietary phosphate, vitamin-D and other hormones stimulate FGF23
142 transiently within a narrow physiologic range[38]. In contrast, CKD and XLH patients have chronically
143 highly elevated FGF23 levels[18,19,21,22,38]. The differential effects of low-transitory (~physiological) versus
144 high-prolonged (~pathological) FGF23 levels on temporal phases of ERK activation are unclear.
145 Continued FGF23 availability for FGFR-Klotho binding in the kidney may lead to sustained-ERK activity,
146 but this has not been demonstrated yet. Sustained-ERK activation regulates several transcription
147 factors and gene signatures that govern inflammation and immune responses[39,40]. We hypothesize that
148 chronically elevated FGF23 levels may cause inflammation and immune gene signatures via sustained-
149 ERK signaling, expanding from the canonical role of FGF23 as a regulator of mineral metabolism.
150
151 **RESULTS**
152 **1. Chronically elevated FGF23 levels in mice induce sustained-ERK signaling, inflammation**
153 **and immune gene signatures in the kidneys, which are mitigated by cFGF23 gene therapy.**
154 An adeno-associated virus (AAV) vector was generated to secrete human cFGF23 from the liver and
155 increase circulating cFGF23 (AAV-cFGF23)[17]. Fig. 1A illustrates the experimental approach used in this
156 study. As expected, serum FGF23 levels in Hyp-Duk mice were significantly higher than in WT mice
157 (Fig. 1B). Circulating human cFGF23 levels were significantly increased in AAV-cFGF23-treated Hyp-
158 Duk mice (Fig. 1C), while this assay did not detect endogenous mouse cFGF23 due to species
159 specificity (Fig. S1). RNA-seq was performed on kidney samples of WT, Hyp-Duk and Hyp-Duk mice
160 treated with AAV-cFGF23 (cFGF23-Hyp-Duk).
161
162 The number of DEGs (p-value<0.05) in the kidneys of Hyp-Duk and cFGF23-Hyp-Duk are shown in
163 Fig. S2 (tables S1/2). Volcano plots illustrate DEGs between the kidneys of Hyp-Duk versus WT and
164 AAV-cFGF23-Hyp-Duk versus Hyp-Duk mice (Fig. 1D). Notably, many canonical FGF23 targets, such
165 as *Dnase1*, *Slc34a1*, *Kl*, and *Ace2*, were downregulated in the kidney of Hyp-Duk mice but upregulated
166 in the kidneys of cFGF23-Hyp-Duk mice, validating the gene therapy approach (Fig. 1D). Previously
167 unrecognized ERK and inflammatory targets, such as *Etv4*, *Stat3*, *Ets1*, and *Nfkb2*, were significantly
168 upregulated in the kidneys of Hyp-Duk mice but downregulated the kidneys of cFGF23-Hyp-Duk mice
169 (Fig. 1D). Notably, only late-ERK targets were significantly upregulated in the kidneys of Hyp-Duk mice
170 and completely or partially rescued in the kidneys of cFGF23-Hyp-Duk mice (Fig. 1E/S3). Early-ERK
171 targets remained unchanged in the kidneys of Hyp-Duk mice (Fig. 1F).
172
173 To determine whether sustained FGF23 signaling alters the renal immune cell landscape, we performed
174 bulk deconvolution of our renal RNA-seq data using reference kidney single-cell transcriptomes. The
175 fraction of transcriptome-inferred immune-like cells was increased in the kidneys of Hyp-Duk mice
176 compared with controls (Fig. 1G). In contrast, cFGF23 overexpression significantly reduced the
177 immune-like cell fraction (Fig. 1G). Further, we intersected DEGs from Hyp-Duk kidneys with the
178 immunological database ImmPort. We found that 20.5% of all DEGs corresponded to ImmPort-
179 annotated genes (Fig. S4; left panel). Notably, cFGF23 gene therapy rescued 27.4% of these affected
180 DEGs (Fig. S4; right panel), which are highlighted in the heatmap (Fig. 1H). GO enrichment analysis
181 identified 277 pathways significantly upregulated (padj < 0.05) in Hyp-Duk kidneys and rescued in

cFGF23-Hyp-Duk kidneys (tables S3/4/5). Many of these pathways were related to inflammation and immune responses. For example, ERK-mediated *Ras signaling*, *inflammatory and immune responses*, *Wnt signaling*, and *complement activation* were significantly upregulated in Hyp-Duk kidneys and rescued by cFGF23 gene therapy (Fig. 1I; tables S3/4/5). In contrast, the inflammatory *JAK-STAT cascade* and *TNF cytokine production* were significantly upregulated and only partially rescued (Fig. 1I; tables S3/4/5). This list is not exhaustive; the full table is provided in tables S3/4/5.

Fig. 1J/K show selected genes implicated in inflammatory and immune gene signatures that were upregulated in the kidneys of Hyp-Duk mice and reversed in the kidneys of cFGF23-Hyp-Duk mice. Genes involved in paracrine FGF signaling, such as *Fgf10*, *Hspg2*, and *Fgf2*, were significantly upregulated in the kidneys of Hyp-Duk mice and rescued in the kidneys of cFGF23-Hyp-Duk mice (Fig. S5). We found canonical mineral metabolism targets of FGF23 in the kidneys of Hyp-Duk mice, such as *Cyp27b1*, *Cyp24a1*, *Slc34a1*, and *Kl*, as well as several previously unrecognized gene targets, including *Slc34a2*, *Pth1r*, and *Calb1* (Fig. S6). Fig. S7 summarizes the pathways upregulated in the renal transcriptional signature associated with skeletal defects in Hyp-Duk mice. *Lcn2* upregulation in Hyp-Duk kidneys prompted us to measure urinary neutrophil gelatinase-associated lipocalin (NGAL), a marker of kidney inflammation and injury. Urinary NGAL levels were significantly elevated in Hyp-Duk mice and were rescued following AAV-cFGF23 treatment (Fig. 1L).

2. Sustained-ERK activation in vitro is induced by prolonged high, but not acute low, FGF23 concentrations.

HEK293 (HEK^{Wt}) cells endogenously express FGFR1-4 but not Klotho. We stably transfected these cells with Klotho to generate a stable Klotho HEK293 cell line (HEK^{Kl}). HEK^{Wt} and HEK^{Kl} cells are excellent models for studying Klotho-independent and Klotho-dependent FGF23 functions, respectively[13,41]. The activation of pERK1/2 by FGF23 in the presence of Klotho was confirmed (Fig. S9). Treatment with 0.5 nM FGF23, which resembles the physiological condition, in HEK^{Kl} cells, resulted in a transient increase in pERK1/2 that was visible after 15 minutes but not at 24 hours (Fig. 2A, left panel). Treatment with 10 nM FGF23, a higher concentration mimicking the pathological levels, led to pERK1/2 activation at 15 minutes which persists to 24 hours (Fig. 2A, right panel). FGF23 concentrations exceeding 5 nM resulted in sustained pERK1/2 activation (Fig. 2B). To determine the precise time points for the transcriptomics analysis, we used both low and high FGF23 concentrations and measured *EGR1* mRNA as a canonical marker for FGF23 signaling. Upon 0.5 nM FGF23 treatment in HEK^{Kl} cells, *EGR1* mRNA peaked at 1 hour, with no statistically significant difference at 24 hours compared to the control HEK^{Wt}-treated cells (Fig. 2C). Notably, 10 nM FGF23 treatment followed almost a similar trend except a 13-fold higher *EGR1* levels were still observed after 24 hours (Fig. 2D/E). Both pERK1/2 and *EGR1* levels remained unchanged in HEK^{Wt} cells throughout the treatment periods indicating the absolute requirement of the co-receptor Klotho for FGF23 signaling.

3. Chronically elevated FGF23 levels induce sustained-ERK signaling and inflammation-related gene signatures *in vitro*.

222 To evaluate the transcriptomic profile after treatment with physiological or pathological FGF23
223 concentrations, we performed RNA-seq analysis as illustrated in Fig. 3A. Physiological FGF23
224 treatment in HEK^{Wt} cells did not affect the transcriptome (Fig. 3B, left panel; table S6; and Fig. S10A).
225 Physiological FGF23 treatment in HEK^{Kl} cells led to 64 differentially expressed genes (DEGs), with 61
226 upregulated and 3 downregulated (Fig. 3B, right panel; table S7). Canonical early genes such as *EGR1,*
227 *FOS* and *JUNB* were among the top upregulated genes, validating our approach. Although pathological
228 FGF23 concentrations in HEK^{Wt} cells resulted in few DEGs, these showed log2FC<1, suggesting a
229 minimal non-Klotho-dependent effect of FGF23 (Fig. 3C, left panel; table S8). While pathological FGF23
230 treatment in HEK^{Kl} cells demonstrated a robust transcriptomics response (Fig. 3C, right panel; table
231 S9).
232
233 The physiological and pathological FGF23 treatments in HEK^{Kl} cells upregulated several ERK target
234 genes (Fig. S11). Early immediate genes like *EGR1, FOS, FOSB, JUNB* and *JUND* were significantly
235 upregulated by physiological FGF23 compared to pathological FGF23 treatment *(early-ERK targets;*
236 Fig. 3D and S11). *EGR1* expression was 150-fold higher after physiological FGF23 treatment, but only
237 10-fold higher in pathological conditions, indicating its primary role in transient-ERK activity. In contrast,
238 *JUNB* and *FOSB* were unchanged by pathological FGF23 treatment, suggesting they are strictly *early-*
239 *ERK targets* (Fig. S11). Conversely, ERK targets such as *DUSP4/6*, *ETV1/4/5*, *SPRED1/2*, and
240 *SPRY2/4* were either unchanged or significantly upregulated by pathological FGF23 compared to
241 physiological FGF23 treatment (Fig. 3E, S12). These transcripts were identified as *late-ERK targets*.
242 Among these, *ETV1/4/5* and *SPRED1/2* were unchanged by physiological FGF23, indicating they are
243 strictly *late-ERK targets* (Fig. S12).
244
245 As depicted in the Venn diagram, 88 and 40 DEGs were exclusively regulated by pathological and
246 physiological FGF23, respectively, with 24 DEGs overlapping (Fig. 3F). This suggests that physiological
247 and pathological FGF23 levels drive divergent transcriptomic responses. Analysis of the Gene ontology
248 (GO) pathways of biological processes linked to genes upregulated by pathological FGF23 identified
249 several processes implicated in inflammation and immune response (Fig. 3G, red arrows. A complete
250 list of GO pathways is available in table S11). Therefore, we intersected DEGs regulated by pathological
251 FGF23 with the immunological database ImmPort (https://www.immport.org). This analysis retrieved a
252 set of genes linked to inflammatory and immune signatures, which are highlighted in the heatmap (Fig.
253 3H). Block 1 of the heatmap shows the inflammatory and immune gene signatures exclusively regulated
254 by pathological FGF23, while block 2 shows genes regulated by both pathological and physiological
255 FGF23. Representative inflammatory and immune gene signatures (*TNFRSF9/12A*, *GDF15*, *ANXA1*,
256 and *TGFB1*) by pathological FGF23 (block 1) are highlighted in Fig. 3I. Notably, the early- and late-ERK
257 targets, as well as novel FGF23 targets implicated in inflammatory and immune gene signatures, are
258 upregulated only in HEK^{Kl} cells and not in HEK^{Wt} cells (Fig. 3I; Fig. S11/S12).
259
260 **4. HEK^{Kl} cells model renal transcriptional programs downstream of FGF23-Klotho signaling.**
261 To determine whether the transcriptomic responses observed *in vitro* recapitulate the renal gene
262 expression changes in Hyp-Duk mice, we compared DEGs implicated between pathological FGF23-

263 treated HEK^{Kl} cells and the kidneys of Hyp-Duk mice. Heatmap analysis of late-ERK targets revealed
264 concordant upregulation of *ETV1*, *ETV4*, *ETV5*, *SPRED2*, *SPRY2*, and *SPRY4* in pathological FGF23-
265 treated HEK^{Kl} cells and their murine orthologs in Hyp-Duk kidneys compared to their respective controls
266 (Fig. 4A). Similarly, genes implicated in inflammatory and immune responses, including *NFKB1*, *RELB*,
267 *STAT3*, *TNFRSF1A*, *CD44*, *MMP2*, *FLI1*, *ITGB1*, *ITGA5*, *ITGA6*, and *BCL2*, were concordantly
268 upregulated in pathological FGF23-treated HEK^{Kl} cells and Hyp-Duk kidneys (Fig. 4B).
269
270 **5. FGF23-mediated inflammatory and immune gene signatures are mediated by FGFR and ERK**
271 ***in vitro.***
272 We used blockers of FGFR (PD173074) and MEK (U0126) to investigate the roles of FGFR and ERK
273 in the effects mediated by pathological FGF23. The mRNA levels of newly identified targets were
274 quantified using qRT-PCR. Pretreatment with either FGFR or MEK inhibitors completely reversed the
275 FGF23-mediated upregulation of the early-ERK target *EGR1* (Fig. 5A, left panel). The late-ERK target
276 *ETV4* was also entirely blocked by the FGFR inhibitor, while it was partially but significantly blocked by
277 the MEK inhibitor (Fig. 5A, right panel). Next, we quantified the inflammation and immune targets such
278 as *TNFRSF9/12A, GDF15, ANXA1,* and *TGFB1*. FGF23-mediated upregulation of mRNA levels of
279 these genes were completely abrogated by FGFR inhibitors and partially but significantly reversed by
280 MEK inhibitors (Fig. 5B). This implies that there is divergence of signaling post FGFR to different
281 pathways.
282
283 **6. cFGF23 mitigates FGF23-mediated inflammatory and immune gene signatures *in vitro*.**
284 The presence of Klotho on the surface was crucial for the transcriptomic response to both physiological
285 and pathological FGF23 levels. To investigate whether FGF23 binding to Klotho was specifically
286 involved in this response, we used recombinant human cFGF23 peptide to prevent FGF23 binding to
287 the FGFR-Klotho co-receptor complex[16] (Fig. 6A). Pretreatment with cFGF23 blocked the FGF23-
288 mediated upregulation of the early-ERK target *EGR1* as well as the late-ERK target *ETV4* in a dose-
289 dependent manner (Fig. 6B). A high dose of cFGF23 (10 μM) alone did not affect *EGR1* mRNA levels;
290 however, it slightly but significantly increased *ETV4* mRNA levels (Fig. 6B, right panel). Next, we
291 validated the inflammation and immune targets such as *TNFRSF9/12A*, *GDF15*, *ANXA1*, and *TGFB1*
292 using qPCR. Similar to ERK targets, FGF23 upregulated these genes, which were partially rescued by
293 cFGF23 co-treatment in a dose-dependent manner (Fig. 6C). Interestingly, cFGF23 alone did not affect
294 the mRNA expressions of any of the inflammatory and immune targets, suggesting that potential "off-
295 target" effects of cFGF23 are probably limited to *ETV4* mRNA (Fig. 6C).
296
297 **DISCUSSION:**
298 Our study provides three salient findings: ***(i)*** chronically elevated FGF23 levels in mice induce
299 sustained-ERK activation and inflammation in the kidney; ***(ii)*** cFGF23 gene therapy mitigates sustained-
300 ERK signaling and associated inflammatory responses by blocking FGFR-Klotho binding; and ***(iii)***
301 FGF23 levels drive temporal ERK signaling dynamics *in-vitro*, with acute physiological levels triggering

transient-ERK activation and chronic pathological levels inducing sustained-ERK activation and inflammatory gene signatures.

We found that the early-ERK targets were unchanged in the kidneys of Hyp-Duk mice, while the Hyp-Duk kidneys exhibited elevated late-ERK targets (sustained-ERK signaling) along with activation of inflammatory and immune signaling pathways. The structurally related isoforms, ERK1 and ERK2, were the first MAPKs identified, based on early observations of their rapid and reversible phosphorylation in response to growth factor stimulation[42]. Activated ERK translocates into the nucleus and stimulates transcription factors associated with immediate early genes (*Egr*, *Fos*, and *Jun* families)[43–45]. This type of transient-ERK activation is known to participate in FGF23-mediated mineral homeostasis in the kidney[7,8,46,47]. Conversely, chronically high FGF23 levels in Hyp-Duk mice elevated late-ERK targets (*Etv*, *Spred*, *Spry* families) likely due to continuous and irreversible translocation of ERK into the nucleus. The sustained-ERK signaling is known to trigger inflammatory and immune responses by activating transcription factors like Nuclear Factor kappa-light-chain-enhancer of activated B cells (NF-κB), ETS-like gene 1 (Elk1), cAMP response element-binding protein (CREB), Signal transducers and activators of transcription (STAT)[39,40,48]. Consistently, genes associated with inflammatory and immune cell infiltration, including *Adgre1* (F4/80), *Ptprc* (CD45), and *H2-Aa* (MHC-II), were significantly upregulated in the kidneys of Hyp-Duk mice and may contribute to the proinflammatory responses. Future studies integrating spatial and protein-level analyses will further refine the mechanistic framework proposed here.

Our findings are consistent with recent elegant single-cell transcriptomic analyses demonstrating Klotho-dependent FGF23 bioactivity in discrete nephron segments and its association with inflammatory gene programs[49]. Present study extends these observations by identifying sustained ERK activation as a mechanistic driver of proinflammatory transcriptional responses under elevated FGF23 conditions and demonstrates that these effects can be mitigated through cFGF23 gene therapy.

Renal NGAL expression and its urinary levels, a marker of kidney injury and inflammation, were significantly elevated in Hyp-Duk mice and were rescued by cFGF23 gene therapy. Classical fibrosis markers, such as *Col1a1* and *Col3a1*, were also upregulated, whereas the conventional kidney injury marker *Havcr1* (KIM-1) was not elevated (table S1), suggesting subclinical kidney injury. Consistently, as reported in prior studies, plasma BUN and creatinine levels were unchanged in Hyp mice[50,51]. This implies that elevated FGF23 alone is probably inadequate to cause renal insufficiency without a second hit, such as aging, hypertension, hyperphosphatemia, uremia, or other CKD-related factors. While this manuscript was in preparation, Bockmann and colleagues reported significant renal comorbidities in pediatric XLH patients, including reduced eGFR and elevated urinary markers of glomerular and tubular injury and inflammation[52]. Both XLH patients and mouse models with elevated FGF23 may exhibit subclinical or undetected kidney injury driven by sustained-ERK signaling and associated inflammation.

The convergence of sustained-ERK and inflammatory gene signatures across HEK^{Kl} cells and Hyp-Duk kidneys supports the notion that elevated FGF23-FGFR-Klotho signaling in HEK^{Kl} cells recapitulates,

at least in part, the renal transcriptional program observed in Hyp-Duk mice. Despite HEK293 cells being a transformed, non-renal cell line, the transcriptomic response to pathological FGF23 was conserved. This is consistent with recent single-cell transcriptomic study demonstrating that Klotho-dependent FGF23 signaling in HEK^{Kl} cells recapitulates key renal transcriptional programs, including MAPK activation and inflammatory gene induction[49]. Given the absence of renal cell models with native Klotho, HEK^{Kl} offers as a tractable in vitro system to model renal FGF23-FGFR-Klotho transcriptomics, while acknowledging inherent differences between transformed cell lines and native nephron segments. Notably, the newly identified proinflammatory FGF23 signaling targets in HEK^{Kl} cells (*TGFB1, TNFRSF9/12A8, ANXA19,* and *GDF1510*) are also elevated in human CKD patients[53–56]; however, whether their in vivo induction reflects FGF23 signaling or secondary inflammatory effects remains unclear.

MEK inhibitor rescued FGF23-mediated sustained-ERK signaling as well as inflammatory and immune gene signatures. FGFR inhibitor completely abolished ERK signaling and inflammatory gene signatures. Both Klotho and FGFRs are expressed in renal proximal and distal tubules, participating in the canonical effects of FGF23 in mineral metabolism[10,11,57,58]. FGFR1/3/4 are implicated in FGF23-Klotho signaling[6,13]. Notably, only FGFR4 was significantly downregulated, while FGFR1/3 remained unchanged in the kidneys of Hyp-Duk mice (Fig. S8). The specific FGFRs mediating the inflammatory FGF23-ERK signaling is presently unclear. Previous studies have shown that both FGFR and ERK inhibition in Hyp mice corrected mineral metabolism and skeletal phenotype[47,59]. It is tempting to speculate that these inhibitors might also block the inflammatory gene signatures triggered by FGF23-mediated sustained-ERK signaling in the kidneys.

A hallmark of our study is that cFGF23 mitigates FGF23-mediated sustained-ERK signaling, and inflammatory gene signatures both *in vitro* and *in vivo*. In Hyp-Duk mice, AAV-cFGF23 treatment led to high levels of human cFGF23 in mouse serum, effectively correcting inflammatory and immune gene signatures. The structure of the FGF23-FGFR-Klotho complex shows that the C-terminal region of FGF23 binds into an extended groove between the Kl1 and Kl2 domains of Klotho[6,13]. The isolated cFGF23 peptide can bind specifically into this groove, competitively inhibiting Klotho-dependent FGF23 signaling[16]. Thus, cFGF23 likely mitigated Klotho-dependent FGF23 actions in Hyp-Duk mice. Supporting our findings, a previous study showed no change in inflammation-related gene expression in the heart and liver of Hyp mice, where Klotho is not expressed[33]. These findings corroborate our *in vitro* data, concluding Klotho is needed for FGF23 signaling. There was no significant transcriptomic response to FGF23 in HEK^{Wt} cells, and ERK activation and inflammatory/immune gene signatures were observed only in HEK^{Kl} cells. These findings largely align with recent studies demonstrating that Klotho is essential for FGF23 signaling[6,13,49]. On the other hand, elevated FGF23 levels were previously shown to trigger inflammation in extrarenal cells such as immune cells and hepatocytes, independent of Klotho[26,28–30]. At present our findings cannot refute Klotho-independent FGF23 actions in inflammation[20,41]. Moreover, recent studies demonstrating direct biological actions of cFGF23 peptides

during inflammation underscore the evolving and context-dependent complexity of FGF23 cleavage biology[60].

The FGF23-mediated proinflammatory sustained-ERK signaling proposed here may have significant implications in human CKD. Preclinical studies suggest that MEK Inhibitor ameliorates CKD by suppressing ERK signaling[61–63]. It remains to be investigated whether the effect was specifically due to blocking FGF23-mediated sustained-ERK signaling. Our study suggests that the beneficial effects of MEK inhibitor in CKD, at least partly, are mediated by blocking FGF23-mediated sustained-ERK pathway. Importantly, recent studies demonstrated that cFGF23 treatment could improve anemia, heart function and some kidney functions in murine models of CKD[23,64,65]. Gene therapy with AAV-cFGF23 may provide a better efficacy due to its known capacity to release steady levels of cFGF23 in circulation without the peak-and-trough effect known to be associated with protein therapy[17].

In conclusion, we propose a model (Fig. 6) in which, pathologically elevated FGF23 levels trigger inflammatory and immune gene signatures through the FGFR-Klotho complex and sustained-ERK activation. These untoward effects of FGF23 were significantly mitigated by cFGF23 gene therapy, warranting further investigation to confirm its clinical potential.

MATERIALS AND METHODS

All the chemicals were purchased from Sigma Aldrich unless otherwise stated.

Culture of HEK293 cells.

HEK293 cell line (HEK^{Wt}) was originally purchased from ATCC. The cells were cultured in a growth medium consisting of Minimum Essential Medium MEM, with L-Glutamine (gibco; Cat #11095-080) supplemented with 10% heat-inactivated FBS and 100 U/ml penicillin, and 100 µg/ml streptomycin (gibco; Cat. #15140122). Cells between passages 6 and 17 were used in this study.

Generation of $HEK293^{Kl}$ cells.

For deriving a stable Klotho cell line, HEK^{Wt} cells were transfected with 3 µg of plasmid DNA (Addgene; Cat #17712; http://n2t.net/addgene:17712; RRID:Addgene_17712) in 60 mm culture dish using Jetprime (Polyplus; Cat #55-134) transfection reagent following manufacturer's protocol. Cells stably expressing Klotho (HEK^{Kl}) were selected using 400 µg/ml of G418. Subsequently, stably expressing Klotho (HEK^{Kl}) cells were expanded and tested for Klotho protein and mRNA expression by immunoblotting and qPCR respectively. Then HEK^{Kl} aliquots were frozen at -150°C until further use.

FGF23 treatments in HEK cells

Both HEK^{Wt} and HEK^{Kl} cells undergo exactly similar experimental conditions. A similar number of HEK^{Wt} and HEK^{Kl} cells were seeded in a 6-well plate. After 48 hours, the cells were serum-starved for 16 hours and treated with either PBS or human recombinant FGF23 (Biotechne; Cat #2604-FG/CF) dissolved in PBS. For RNA-seq analysis, following two protocols were applied:

Physiological FGF23 treatment: HEK^{Wt} and HEK^{Kl} cells were treated with 0.5 nM FGF23 or control (PBS) for 1 hour.

Pathological FGF23 treatment: HEK^{Wt} and HEK^{KI} cells were treated with 10 nM FGF23 or control (PBS) for 24 hours. After each experiment, cells were washed with ice-cold PBS, and RNA was isolated as mentioned elsewhere.

Treatment with FGFR/ERK inhibitor and cFGF23 peptide

Forty-eight hours after seeding HEK^{KI} cells in a 6-well plate, the cells were serum-starved for 16 hours and pretreated with 100 nM FGFR inhibitor PD173074 (Biotechne; Cat #3044/10) or 5 µM MEK inhibitor U0126 (Biotechne; Cat #1144/5) for 1 hour. Then, the treatment was continued for the next 24 hours with 10 nM FGF23 or control (PBS). Isolated cFGF23 peptide[16] (1, 5, 10 µM) was similarly pretreated for 1 hour and then continued with 10 nM FGF23 for 24 hours.

Animal experiments

The animal studies were performed according to French and European legislation on animal care and experimentation (2010/63/EU) and were approved by the local Institutional Ethical Board (protocol number 2019-004). In short, the Hyp-Duk mice were obtained from the Jackson Laboratory (Bar Harbor, ME). The treatment consisted of an intravenous injection of AAV-cFGF23 administered at a dose of 1×10^{12} vg per mouse at 4 weeks of age[17]. The experiment included three groups of mice: PBS-treated WT mice (WT, PBS), PBS-treated Hyp-Duk−/0 mice (Hyp-Duk, PBS), and AAV-cFGF23–treated Hyp-Duk−/0 mice (Hyp-Duk, AAV-cFGF23). Mice were sacrificed after 3 months after intravenous injections of AAV-cFGF23.The cloning of the FGF23 constructs and AAV vector production are described[17]. Urinary NGAL in spot urine samples was measured using a commercial ELISA kit (R&D, Cat. #MLCN20) and normalized to creatinine, measured by the Jaffe method.

To test the species specificity of different FGF23 assays, serum from three male wild-type C57Bl/6 mice (2-3 months old) was spiked with human recombinant FGF23. The FGF23 levels were measured using mouse intact-FGF23 (Quidel, Cat. #60-6800), mouse c-terminal FGF23 (Quidel, Cat. #60-6300), human c-terminal FGF23 (Quidel, Cat. #60-6100) ELISA kits according to the manufacturer's instructions. We found that only the human cFGF23 ELISA was species-specific and did not detect endogenous mouse FGF23 fragments (Fig. S1B). Both mouse cFGF23 and iFGF23 assays showed cross-reactivity with human FGF23 fragments (Fig. S1C/D).

Immunoblotting

Both HEK^{Wt} and HEK^{KI} cells were homogenized in ice-cold RIPA lysis buffer (Thermo Fisher, Cat. #89900) containing protease and phosphate inhibitors. Then cell lysates were centrifuged for 10 min at 2000 g and supernatants were used for immunoblotting. Protein concentration was measured by Bradford assay (CooAssay Protein Dosage Reagent; Uptima, Cat. #UPF86421). Equal amounts of protein (30 µg) were loaded in Laemmli buffer (pH 6.8) on 8% polyacrylamide gels. Electrophoretically separated proteins were blotted to nitrocellulose membranes at 100 V for 2 hours. Next, membranes were blocked in Odyssey blocking buffer (LI-COR; Cat. # 927-70001) for 1 hour. The membrane was further incubated with diluted anti-human Klotho monoclonal antibody/Clone: KM2076 (TransGenic; Cat. #KO603), pERK1/2 (Cell Signaling; Cat #4370S) and tERK1/2 (Cell Signaling; Cat. #4695S)

overnight at 4°C. On the following day, diluted secondary antibodies goat-anti-rabbit IRDye 800 (LI-COR; Cat. #926-32211), goat-anti-rat IRDye 800 (LI-COR; Cat. #926-32219) and goat-anti-mouse IRDye 680 (LI-COR; Cat. #926-68070) were added to the membranes in Casein Blocking solution in deionized water (1:10) and incubated for 1 hour at room temperature. Then membranes were repeatedly washed with phosphate-buffered saline containing 0.1% Tween 20. The fluorescent signal was visualized using Odyssey IR imaging system (LI-COR Biosciences).

RNA isolation and qRT-PCR

The RNA was extracted from HEK^{Wt} and HEK^{Kl} cells using a Nucleospin RNA isolation kit (Macherry Nagel; Cat. #740955). The RNA was transcribed using a High-Capacity cDNA Reverse Transcription Kit (Thermo Fisher; Cat. #4374966) and subjected to qPCR with SybrGreen Master Mix (Roche; Cat. #4707516001) using the following primers:

hKL-Fwd: GCTTTCCTGGATTGACCTTG
hKL-Rev: TGTAACCTCTGTGCCACTCG

hEGR1-Fwd: AGAAGGACAAGAAAGCAGACAAAAGTGT
hEGR1-Rev: GGGGACGGGTAGGAAGAGAG

hETV4-Fwd: TGGAGAGCAGTGCCTTTACTC
hETV4-Rev: TTGATGGCGATTTGTCTGGGG

hTGFB1-Fwd: GCCACAGATCCCCTATTCAA
hTGFB1-Rev: GTCTCAGTATCCCACGGAAA

hTNFRSF9-Fwd: TCTTCCTCACGCTCCGTTTCTC
hTNFRSF9-Rev: TGGAAATCGGCAGCTACAGCCA

hTNFRSF12a-Fwd: CCAAGCTCCTCCAACCACAA
hTNFRSF12a-Rev: TGGGGCCTAGTGTCAAGTCT

hGDF15-Fwd: GAGCTGGGAAGATTCGAACA
hGDF15-Rev: AGAGATACGCAGGTGCAGGT

hGAPDH-Fwd: ACAACTTTGGTATCGTGGAAGGAC
hGAPDH-Rev: CAGGGATGATGTTCTGGAGAG

The relative quantification of gene expression based on double-delta Ct (threshold cycle) analysis was performed after normalization to *GAPDH* expression. All the gene expression values are expressed as arithmetic means ± SD, where n represents a number of independent experiments (biological replicates). An unpaired Student's t-test was used for comparisons between the groups using GraphPad Prism.

RNA-sequencing and data analysis

RNA-seq was performed by a commercial vendor (Novogene Company Limited, UK) as previously described[3]. In brief, amplified cDNA samples were subjected to different quality control standards. RNA

513 sample was used for library preparation using NEB Next® Ultra RNA Library Prep Kit for Illumina®.
514 Indices were included to multiplex multiple samples. Briefly, mRNA was purified from total RNA using
515 poly-T oligo-attached magnetic beads. After fragmentation, the first strand cDNA was synthesized using
516 random hexamer primers followed by the second strand cDNA synthesis. The library was ready after
517 end repair, A-tailing, adapter ligation, and size selection. After amplification and purification, the insert
518 size of the library was validated on an Agilent 2100 and quantified using quantitative qPCR. Libraries
519 were then sequenced on Illumina NovaSeq 6000 S4 flow cell with PE150 according to results from
520 library quality control and expected data volume. Differential expression analysis of experimental groups
521 (with different biological replicates per group) was performed using the DESeq2 R package (1.20.0).
522 The resulting p-values were adjusted using the Benjamini and Hochberg's approach for controlling the
523 false discovery rate. Genes with a padj/p-value<0.05 found by DESeq2 were assigned as differentially
524 expressed. GO enrichment analysis of DEGs was implemented by the clusterProfiler R package. GO
525 terms with padj less than 0.05 were considered significantly enriched by DEGs. Venn diagrams for the
526 sets of genes up- or down-regulated were made by intersecting the lists of gene names between control
527 and FGF23 treatment.
528
529 We included 24 tables for *in vitro* RNA-Seq data analysis, three biological replicates in each group. List
530 of eight experimental groups as follows: (1) KI_FGF23_1h; (2) KI_Ctrl_1h; (3) WT_FGF23_1h; (4)
531 WT_Ctrl_1h; (5) KI_FGF23_24h; (6) KI_Ctrl_24h; (7) WT_FGF23_24h; (8) WT_Ctrl_24h. For *in vivo*
532 RNA-Seq data analysis, five mice in each group were included with three experimental groups as
533 follows: (1) WT; (2) Hyp-Duk; (3) cFGF23-Hyp-Duk. The following thresholds for DEGs were applied:
534 padj<0.05 for *in vitro* data and p-value<0.05 for *in vivo* data. This was due to larger biological variations
535 in mice and the inclusion of five mice per group in the *in vivo* study, compared to three samples per
536 group in the *in vitro* study.
537
538 *Analysis of immune related genes*
539 For the analysis of immune-related genes differentially expressed due to pathological FGF23 treatment
540 *in vitro*, we retrieved a list of curated genes from the InnateDB website (https://www.innatedb.com),
541 which corresponds to a set of genes derived from the Immunology Database and Analysis Portal
542 (ImmPort). Briefly, we intersected the ImmPort gene list with the DEGs from pathological FGF23
543 treatment in HEK^{KI} cells (padj<0.05 and abs(log2FC)>1) and used the retrieved gene set for heatmap
544 representation. A similar analysis was performed for the *in vivo* data by translating the ImmPort human
545 genes to their mouse orthologs using biomaRt (version 2.44.4) and intersecting the list with the set of
546 DEGs between Hyp-Duk and WT mice (p-value<0.05). The proportions of immune-related genes
547 rescued by AAV-cFGF23 treatment were obtained by identifying genes overlapping with the ImmPort
548 list that were significantly regulated (p-value<0.05) in opposite directions for the comparisons Hyp-Duk
549 vs. WT and cFGF23-Hyp-Duk vs. Hyp-Duk. The normalized expression values for WT, Hyp-Duk and
550 cFGF23-Hyp-Duk were used for the heatmap.
551
552 *Analysis of biological processes recovered upon AAV-cFGF23 treatment in vivo*
553 For the analysis of GO terms rescued after AAV-cFGF23 treatment, we first retrieved the list of
554 significantly enriched GO terms (padj<0.05) linked to upregulated genes (p-value<0.05) for the

comparison of Hyp-Duk vs. WT. The output list was then intersected with the list of enriched GO terms linked to downregulated genes for the cFGF23-Hyp-Duk vs. Hyp-Duk. Representative GO terms included in the intersected output were selected for the barplot representation.

Deconvolution analysis:

Single-cell RNAseq dataset GSE107585 of murine kidney from 7 sex-mixed healthy C57BL/6 mice by Park et al. was downloaded from Gene Expression Omnibus. Using Seurat v 5.3, we excluded cells with less than 200 or more than 2500 features and cells with >5% mitochondrial RNA content. Following normalization and clustering, clusters were annotated based on markers with reference to the original dataset description (Park et al., Science 2018). Bisque v.1.0.5 was then used for deconvolution in reference-based decomposition mode.

Statistics

All the values are expressed as arithmetic means ± SEM, where n represents number of independent experiments (biological replicates). An unpaired Student's t test was used for comparisons between the groups using GraphPad Prism. In cases where the p value is not mentioned, the following applies: ns (not significant) $p > 0.05$, $*p \leq 0.05$, $**p < 0.01$, and $***p < 0.001$.

Illustrations

Graphical illustrations were created using a licensed version of Biorender software.

DATA AVAILABILITY

All the relevant data associated with the current study can be found in the main text or supplementary tables. The raw RNA-seq data used in this publication have been deposited in NCBI Gene Expression Omnibus and are accessible through GEO series accession numbers GSE248734 and GSE269823. All data are available from the authors upon reasonable request.

ACKNOWLEDGMENTS

This work was supported by the Swiss National Science Foundation through the National Center of Competence in Research NCCR Kidney.CH (N-403-03-55 to G.P.), City University of Hong Kong (9610769 to G.P.), Clinical Research Priority Program HYpertension REsearch NEtwork (CRPP HYRENE) of the University of Zurich (to J. L.), National Natural Science Foundation of China (82073705 & 82273842 to G.C.), Natural Science Foundation for International Senior Scientists (32350710196 to M.M.), Oujiang laboratory startup fund (OJQD2022007 to M.M.), Kungpeng Action Plan award (to M.M.), Natural Science Funding of Zhejiang Province (LR22H300002 to G.C.). The authors thank Prof. Orson Moe and Johanne Pastor from the University of Texas Southwestern Medical Center, Dallas, Texas, USA, for their critical feedback on the manuscript.

AUTHORS CONTRIBUTIONS

GP conceptualized the study; ASB, CB, GR and GP designed the study; ASB, CB, KK, LJ, FC, AF and GP performed the study; GC, MM and JL contributed new reagents/analytic tools; ASB, CB, KK, LJ, FC, AF GC, MM, CS, LS, JL, GR and GP analyzed the data; GP wrote the manuscript; ASB, CB, KK,

LJ, FC, AF GC, MM, CS, LS, JL and GR reviewed and edited the manuscript; GP and JL were responsible for funding acquisition; GP was responsible for supervision.

625 **REFERENCES**

626 1. Feng, J. Q., Ward, L. M., Liu, S., Lu, Y., Xie, Y., Yuan, B., Yu, X., Rauch, F., Davis, S. I., Zhang, S., Rios, H., Drezner, M. K.,
627 Quarles, L. D., … White, K. E. Loss of DMP1 causes rickets and osteomalacia and identifies a role for osteocytes in
628 mineral metabolism. *Nat Genet* **38**, 1310–1315 (2006).

629 2. Shimada, T., Mizutani, S., Muto, T., Yoneya, T., Hino, R., Takeda, S., Takeuchi, Y., Fujita, T., Fukumoto, S. & Yamashita,
630 T. Cloning and characterization of FGF23 as a causative factor of tumor-induced osteomalacia. *Proc Natl Acad Sci U*
631 *S A* **98**, 6500–6505 (2001).

632 3. Radvanyi, Z., Yoo, E. J., Kandasamy, P., Salas-Bastos, A., Monnerat, S., Refardt, J., Christ-Crain, M., Hayashi, H.,
633 Kondo, Y., Jantsch, J., Rubio-Aliaga, I., Sommer, L., Wagner, C. A., … Pathare, G. Extracellular sodium regulates
634 fibroblast growth factor 23 (FGF23) formation. *J Biol Chem* 105480 (2023) doi:10.1016/J.JBC.2023.105480.

635 4. Shimada, T., Hasegawa, H., Yamazaki, Y., Muto, T., Hino, R., Takeuchi, Y., Fujita, T., Nakahara, K., Fukumoto, S. &
636 Yamashita, T. FGF-23 is a potent regulator of vitamin D metabolism and phosphate homeostasis. *Journal of Bone*
637 *and Mineral Research* **19**, 429–435 (2004).

638 5. Urakawa, I., Yamazaki, Y., Shimada, T., Iijima, K., Hasegawa, H., Okawa, K., Fujita, T., Fukumoto, S. & Yamashita, T.
639 Klotho converts canonical FGF receptor into a specific receptor for FGF23. *Nature* **444**, 770–774 (2006).

640 6. Chen, L., Fu, L., Sun, J., Huang, Z., Fang, M., Zinkle, A., Liu, X., Lu, J., Pan, Z., Wang, Y., Liang, G., Li, X., Chen, G. &
641 Mohammadi, M. Structural basis for FGF hormone signalling. *Nature* **618**, 862–870 (2023).

642 7. Portale, A. A., Zhang, M. Y. H., David, V., Martin, A., Jiao, Y., Gu, W. & Perwad, F. Characterization of FGF23-
643 Dependent Egr-1 Cistrome in the Mouse Renal Proximal Tubule. *PLoS One* **10**, e0142924 (2015).

644 8. Ni, P., Clinkenbeard, E. L., Noonan, M. L., Richardville, J. M., McClintick, J., Hato, T., Janosevic, D., Cheng, Y. H., El-
645 Achkar, T. M., Eadon, M. T., Dagher, P. C. & White, K. E. Targeting fibroblast growth factor 23-responsive pathways
646 uncovers controlling genes in kidney mineral metabolism. *Kidney Int* **99**, 598–608 (2021).

647 9. Lindberg, K., Amin, R., Moe, O. W., Hu, M.-C., Erben, R. G., Östman Wernerson, A., Lanske, B., Olauson, H. &
648 Larsson, T. E. The Kidney Is the Principal Organ Mediating Klotho Effects. *Journal of the American Society of*
649 *Nephrology* **25**, 2169–2175 (2014).

650 10. Bourqui, L., Trnjanin, A., Kopper, K., Loffing-Cueni, D., Radvanyi, Z., Karpovich, A., Rahimi, T., Santos, R., Wengi, A.,
651 Pastor, J., Moe, O. W., Loffing, J. & Pathare, G. Klotho in the kidney distal convolution regulates urinary Klotho
652 excretion and kidney calcium reabsorption, but not phosphate homeostasis. *Kidney Int* **0**, (2026).

653 11. Kuro-o, M., Matsumura, Y., Aizawa, H., Kawaguchi, H., Suga, T., Utsugi, T., Ohyama, Y., Kurabayashi, M., Kaname, T.,
654 Kume, E., Iwasaki, H., Iida, A., Shiraki-Iida, T., … Nabeshima, Y. I. Mutation of the mouse klotho gene leads to a
655 syndrome resembling ageing. *Nature* **390**, 45–51 (1997).

656 12. Kurosu, H., Yamamoto, M., Clark, J. D., Pastor, J. V., Nandi, A., Gurnani, P., McGuinness, O. P., Chikuda, H.,
657 Yamaguchi, M., Kawaguchi, H., Shimomura, I., Takayama, Y., Herz, J., … Kuro-O, M. Suppression of aging in mice by
658 the hormone Klotho. *Science (1979)* **309**, 1829–33 (2005).

659 13. Chen, G., Liu, Y., Goetz, R., Fu, L., Jayaraman, S., Hu, M. C., Moe, O. W., Liang, G., Li, X. & Mohammadi, M. α-Klotho
660 is a non-enzymatic molecular scaffold for FGF23 hormone signalling. *Nature* **553**, 461–466 (2018).

661 14. White, K. E., Evans, W. E., O'Riordan, J. L. H., Speer, M. C., Econs, M. J., Lorenz-Depiereux, B., Grabowski, M.,
662 Meitinger, T. & Strom, T. M. Autosomal dominant hypophosphataemic rickets is associated with mutations in
663 FGF23. *Nat Genet* **26**, 345–348 (2000).

664 15. Larsson, T., Davis, S. I., Garringer, H. J., Mooney, S. D., Draman, M. S., Cullen, M. J. & White, K. E. FGF23 mutants
665 causing familial tumoral calcinosis are differentially processed. *Endocrinology* **146**, 3883–3891 (2005).

666 16. Goetz, R., Nakada, Y., Hu, M. C., Kurosu, H., Wang, L., Nakatani, T., Shi, M., Eliseenkova, A. V., Razzaque, M. S., Moe,
667 O. W., Kuro-o, M. & Mohammadi, M. Isolated C-terminal tail of FGF23 alleviates hypophosphatemia by inhibiting
668 FGF23-FGFR-Klotho complex formation. *Proc Natl Acad Sci U S A* **107**, 407–412 (2010).

669 17. Zhukouskaya, V. V., Jauze, L., Charles, S., Leborgne, C., Hilliquin, S., Sadoine, J., Slimani, L., Baroukh, B., van
670 Wittenberghe, L., Danièle, N., Rajas, F., Linglart, A., Mingozzi, F., … Ronzitti, G. A novel therapeutic strategy for
671 skeletal disorders: Proof of concept of gene therapy for X-linked hypophosphatemia. *Sci Adv* **7**, (2021).

672 18. Mendoza, J. M., Isakova, T., Ricardo, A. C., Xie, H., Navaneethan, S. D., Anderson, A. H., Bazzano, L. A., Xie, D.,
673 Kretzler, M., Nessel, L., Lee Hamm, L., Negrea, L., Leonard, M. B., … Wolf, M. Fibroblast growth factor 23 and
674 Inflammation in CKD. *Clin J Am Soc Nephrol* **7**, 1155–1162 (2012).

675 19. Wallquist, C., Mansouri, L., Norrbäck, M., Hylander, B., Jacobson, S. H., Larsson, T. E. & Lundahl, J. Associations of
676 Fibroblast Growth Factor 23 with Markers of Inflammation and Leukocyte Transmigration in Chronic Kidney
677 Disease. *Nephron* **138**, 287–295 (2018).

678 20. Faul, C., Amaral, A. P., Oskouei, B., Hu, M. C., Sloan, A., Isakova, T., Gutiérrez, O. M., Aguillon-Prada, R., Lincoln, J.,
679 Hare, J. M., Mundel, P., Morales, A., Scialla, J., … Wolf, M. FGF23 induces left ventricular hypertrophy. *Journal of*
680 *Clinical Investigation* **121**, 4393–4408 (2011).

681 21. Gutiérrez, O. M., Mannstadt, M., Isakova, T., Rauh-Hain, J. A., Tamez, H., Shah, A., Smith, K., Lee, H., Thadhani, R.,
682 Jüppner, H. & Wolf, M. Fibroblast growth factor 23 and mortality among patients undergoing hemodialysis. *N Engl J*
683 *Med* **359**, 584–592 (2008).

684 22. Isakova, T., Xie, H., Yang, W., Xie, D., Anderson, A. H., Scialla, J., Wahl, P., Gutiérrez, O. M., Steigerwalt, S., He, J.,
685 Schwartz, S., Lo, J., Ojo, A., … Wolf, M. Fibroblast growth factor 23 and risks of mortality and end-stage renal
686 disease in patients with chronic kidney disease. *JAMA* **305**, 2432–2439 (2011).

687 23. Hu, M. C., Reneau, J. A., Shi, M., Takahashi, M., Chen, G., Mohammadi, M. & Moe, O. W. C-terminal fragment of
688 fibroblast growth factor 23 improves heart function in murine models of high intact fibroblast growth factor 23.
689 *Am J Physiol Renal Physiol* **326**, F584–F599 (2024).

690 24. Fitzpatrick, E. A., Han, X., Xiao, Z. & Quarles, L. D. Role of fibroblast growth factor-23 in innate immune responses.
691 *Front Endocrinol (Lausanne)* **9**, 372263 (2018).

692 25. Egli-Spichtig, D., Imenez Silva, P. H., Glaudemans, B., Gehring, N., Bettoni, C., Zhang, M. Y. H., Pastor-Arroyo, E. M.,
693 Schönenberger, D., Rajski, M., Hoogewijs, D., Knauf, F., Misselwitz, B., Frey-Wagner, I., … Wagner, C. A. Tumor
694 necrosis factor stimulates fibroblast growth factor 23 levels in chronic kidney disease and non-renal inflammation.
695 *Kidney Int* **96**, 890–905 (2019).

696 26. Masuda, Y., Ohta, H., Morita, Y., Nakayama, Y., Miyake, A., Itoh, N. & Konishi, M. Expression of Fgf23 in Activated
697 Dendritic Cells and Macrophages in Response to Immunological Stimuli in Mice. *Biol Pharm Bull* **38**, 687–693
698 (2015).

699 27. Ito, N., Wijenayaka, A. R., Prideaux, M., Kogawa, M., Ormsby, R. T., Evdokiou, A., Bonewald, L. F., Findlay, D. M. &
700 Atkins, G. J. Regulation of FGF23 expression in IDG-SW3 osteocytes and human bone by pro-inflammatory stimuli.
701 *Mol Cell Endocrinol* **399**, 208–218 (2015).

702 28. Singh, S., Grabner, A., Yanucil, C., Schramm, K., Czaya, B., Krick, S., Czaja, M. J., Bartz, R., Abraham, R., Di Marco, G.
703 S., Brand, M., Wolf, M. & Faul, C. Fibroblast growth factor 23 directly targets hepatocytes to promote inflammation
704 in chronic kidney disease. *Kidney Int* **90**, 985–996 (2016).

705 29. Smith, E. R., Tan, S. J., Holt, S. G. & Hewitson, T. D. FGF23 is synthesised locally by renal tubules and activates
706 injury-primed fibroblasts. *Scientific Reports 2017 7:1* **7**, 1–14 (2017).

707 30. Smith, E. R., Holt, S. G. & Hewitson, T. D. FGF23 activates injury-primed renal fibroblasts via FGFR4-dependent
708 signalling and enhancement of TGF-β autoinduction. *Int J Biochem Cell Biol* **92**, 63–78 (2017).

709 31. Liu, S., Guo, R., Simpson, L. G., Xiao, Z. S., Burnham, C. E. & Quarles, L. D. Regulation of fibroblastic growth factor
710 23 expression but not degradation by PHEX. *Journal of Biological Chemistry* **278**, 37419–37426 (2003).

711 32. Yuan, B., Takaiwa, M., Clemens, T. L., Feng, J. Q., Kumar, R., Rowe, P. S., Xie, Y. & Drezner, M. K. Aberrant Phex
712 function in osteoblasts and osteocytes alone underlies murine X-linked hypophosphatemia. *Journal of Clinical*
713 *Investigation* **118**, 722–734 (2008).

714 33. Pastor-Arroyo, E. M., Gehring, N., Krudewig, C., Costantino, S., Bettoni, C., Knöpfel, T., Sabrautzki, S., Lorenz-
715 Depiereux, B., Pastor, J., Strom, T. M., Hrabě de Angelis, M., Camici, G. G., Paneni, F., … Rubio-Aliaga, I. The
716 elevation of circulating fibroblast growth factor 23 without kidney disease does not increase cardiovascular disease
717 risk. *Kidney Int* **94**, 49–59 (2018).

718 34. Akwo, E., Pike, M. M., Ertuglu, L. A., Vartanian, N., Farber-Eger, E., Lipworth, L., Perwad, F., Siew, E., Hung, A.,
719 Bansal, N., Boer, I. de, Kestenbaum, B., Cox, N. J., … Robinson-Cohen, C. Association of Genetically Predicted

720 Fibroblast Growth Factor-23 with Heart Failure A Mendelian Randomization Study. *Clinical Journal of the American*
721 *Society of Nephrology* **17**, 1183–1193 (2022).

722 35. Leifheit-Nestler, M., Wagner, M. A., Richter, B., Piepert, C., Eitner, F., Böckmann, I., Vogt, I., Grund, A., Hille, S. S.,
723 Foinquinos, A., Zimmer, K., Thum, T., Müller, O. J. & Haffner, D. Cardiac Fibroblast Growth Factor 23 Excess Does
724 Not Induce Left Ventricular Hypertrophy in Healthy Mice. *Front Cell Dev Biol* **9**, 2987 (2021).

725 36. Liu, E. S., Thoonen, R., Petit, E., Yu, B., Buys, E. S., Scherrer-Crosbie, M. & Demay, M. B. Increased Circulating FGF23
726 Does Not Lead to Cardiac Hypertrophy in the Male Hyp Mouse Model of XLH. *Endocrinology* **159**, 2165–2172
727 (2018).

728 37. Meaux, M. N., Alioli, C., Linglart, A., Lemoine, S., Vignot, E., Bertholet-Thomas, A., Peyruchaud, O., Flammier, S.,
729 Machuca-Gayet, I. & Bacchetta, J. X-Linked Hypophosphatemia, Not Only a Skeletal Disease But Also a Chronic
730 Inflammatory State. *J Clin Endocrinol Metab* **107**, 3275–3286 (2022).

731 38. Edmonston, D., Grabner, A. & Wolf, M. FGF23 and klotho at the intersection of kidney and cardiovascular disease.
732 *Nature Reviews Cardiology 2023* 1–14 (2023) doi:10.1038/s41569-023-00903-0.

733 39. Kyriakis, J. M. & Avruch, J. Mammalian MAPK signal transduction pathways activated by stress and inflammation: a
734 10-year update. *Physiol Rev* **92**, 689–737 (2012).

735 40. Cargnello, M. & Roux, P. P. Activation and Function of the MAPKs and Their Substrates, the MAPK-Activated Protein
736 Kinases. *Microbiol Mol Biol Rev* **75**, 50 (2011).

737 41. Grabner, A., Amaral, A. P., Schramm, K., Singh, S., Sloan, A., Yanucil, C., Li, J., Shehadeh, L. A., Hare, J. M., David, V.,
738 Martin, A., Fornoni, A., Di Marco, G. S., … Faul, C. Activation of cardiac fibroblast growth factor receptor 4 causes
739 left ventricular hypertrophy. *Cell Metab* **22**, 1020–1032 (2015).

740 42. Cooper, J. A., Sefton, B. M. & Hunter, T. Diverse mitogenic agents induce the phosphorylation of two related
741 42,000-dalton proteins on tyrosine in quiescent chick cells. *Mol Cell Biol* **4**, 30–37 (1984).

742 43. Chen, R.-H., Sarnecki, C. & Blenis, J. Nuclear localization and regulation of erk- and rsk-encoded protein kinases.
743 *Mol Cell Biol* **12**, 915 (1992).

744 44. Lenormand, P., Sardet, C., Pagès, G., L'Allemain, G., Brunet, A. & Pouysségur, J. Growth factors induce nuclear
745 translocation of MAP kinases (p42mapk and p44mapk) but not of their activator MAP kinase kinase (p45mapkk) in
746 fibroblasts. *J Cell Biol* **122**, 1079–1088 (1993).

747 45. Hazzalin, C. A. & Mahadevan, L. C. MAPK-regulated transcription: a continuously variable gene switch? *Nat Rev Mol*
748 *Cell Biol* **3**, 30–40 (2002).

749 46. Farrow, E. G., Davis, S. I., Summers, L. J. & White, K. E. Initial FGF23-mediated signaling occurs in the distal
750 convoluted tubule. *Journal of the American Society of Nephrology* **20**, 955–960 (2009).

751 47. Ranch, D., Zhang, M. Y., Portale, A. A. & Perwad, F. Fibroblast growth factor 23 regulates renal 1,25-
752 dihydroxyvitamin D and phosphate metabolism via the MAP kinase signaling pathway in Hyp mice. *J Bone Miner*
753 *Res* **26**, 1883–90 (2011).

754 48. Lucas, R. M., Luo, L. & Stow, J. L. ERK1/2 in immune signalling. *Biochem Soc Trans* **50**, 1341–1352 (2022).

755 49. Agoro, R., Myslinski, J., Marambio, Y. G., Janosevic, D., Jennings, K. N., Liu, S., Hibbard, L. M., Fang, F., Ni, P.,
756 Noonan, M. L., Solis, E., Chu, X., Wang, Y., … White, K. E. Dynamic single cell transcriptomics defines kidney
757 FGF23/KL bioactivity and novel segment-specific inflammatory targets. *Kidney Int* **107**, 687–699 (2025).

758 50. Ichikawa, S., Austin, A. M., Gray, A. K. & Econs, M. J. A Phex Mutation in a Murine Model of X-linked
759 Hypophosphatemia Alters Phosphate Responsiveness of Bone Cells. *Journal of Bone and Mineral Research* **27**, 453
760 (2012).

761 51. Sui, T., Yuan, L., Liu, H., Chen, M., Deng, J., Wang, Y., Li, Z. & Lai, L. CRISPR/Cas9-mediated mutation of PHEX in
762 rabbit recapitulates human X-linked hypophosphatemia (XLH). *Hum Mol Genet* **25**, 2661–2671 (2016).

763 52. Böckmann, I., Leifheit-Nestler, M., John, U., Metzing, O., Rehberg, M., Schlingmann, K. P., Weitz, M., Wühl, E.,
764 Sparta, G., Schnabel, D., Hoppe, B. & Haffner, D. #1323 Kidney health in children with X-linked hypophosphatemia:

765 lessons from the prospective multicenter study in Germany and Switzerland. *Nephrology Dialysis Transplantation*
766 **39**, 518–524 (2024).

767 53. Meng, X. M., Nikolic-Paterson, D. J. & Lan, H. Y. TGF-β: the master regulator of fibrosis. *Nature Reviews Nephrology*
768 *2016 12:6* **12**, 325–338 (2016).

769 54. Moreno, J. A., Izquierdo, M. C., Sanchez-Niño, M. D., Suárez-Alvarez, B., Lopez-Larrea, C., Jakubowski, A., Blanco, J.,
770 Ramirez, R., Selgas, R., Ruiz-Ortega, M., Egido, J., Ortiz, A. & Sanz, A. B. The inflammatory cytokines TWEAK and
771 TNFα reduce renal klotho expression through NFκB. *Journal of the American Society of Nephrology* **22**, 1315–1325
772 (2011).

773 55. Wu, L., Liu, C., Chang, D. Y., Zhan, R., Sun, J., Cui, S. H., Eddy, S., Nair, V., Tanner, E., Brosius, F. C., Looker, H. C.,
774 Nelson, R. G., Kretzler, M., … Zheng, L. Annexin A1 alleviates kidney injury by promoting the resolution of
775 inflammation in diabetic nephropathy. *Kidney Int* **100**, 107–121 (2021).

776 56. Nair, V., Robinson-Cohen, C., Smith, M. R., Bellovich, K. A., Bhat, Z. Y., Bobadilla, M., Brosius, F., De Boer, I. H.,
777 Essioux, L., Formentini, I., Gadegbeku, C. A., Gipson, D., Hawkins, J., … Bansal, N. Growth Differentiation Factor-15
778 and Risk of CKD Progression. *J Am Soc Nephrol* **28**, 2233–2240 (2017).

779 57. Hu, M. C., Shi, M., Zhang, J., Pastor, J., Nakatani, T., Lanske, B., Razzaque, M. S., Rosenblatt, K. P., Baum, M. G., Kuro-
780 O, M. & Moe, O. W. Klotho: a novel phosphaturic substance acting as an autocrine enzyme in the renal proximal
781 tubule. *The FASEB Journal* **24**, 3438–3450 (2010).

782 58. Li, H., Martin, A., David, V. & Quarles, L. D. Compound deletion of Fgfr3 and Fgfr4 partially rescues the Hyp mouse
783 phenotype. *Am J Physiol Endocrinol Metab* **300**, (2011).

784 59. Wöhrle, S., Henninger, C., Bonny, O., Thuery, A., Beluch, N., Hynes, N. E., Guagnano, V., Sellers, W. R., Hofmann, F.,
785 Kneissel, M. & Graus Porta, D. Pharmacological inhibition of fibroblast growth factor (FGF) receptor signaling
786 ameliorates FGF23-mediated hypophosphatemic rickets. *J Bone Miner Res* **28**, 899–911 (2013).

787 60. Courbon, G., Thomas, J. J., Martinez-Calle, M., Wang, X., Spindler, J., Von Drasek, J., Hunt-Tobey, B., Mehta, R.,
788 Isakova, T., Chang, W., Creemers, J. W. M., Ji, P., Martin, A. & David, V. Bone-derived C-terminal FGF23 cleaved
789 peptides increase iron availability in acute inflammation. *Blood* **142**, 106–118 (2023).

790 61. Andrikopoulos, P., Kieswich, J., Pacheco, S., Nadarajah, L., Harwood, S. M., O'Riordan, C. E., Thiemermann, C. &
791 Yaqoob, M. M. The MEK Inhibitor Trametinib Ameliorates Kidney Fibrosis by Suppressing ERK1/2 and mTORC1
792 Signaling. *J Am Soc Nephrol* **30**, 33–49 (2019).

793 62. Das, R., Kim, S.-J., Nguyen, N. T., Kwon, H. J., Cha, S.-K. & Park, K.-S. Inhibition of the ERK1/2-mTORC1 axis
794 ameliorates proteinuria and the fibrogenic action of transforming growth factor-β in Adriamycin-induced
795 glomerulosclerosis. *Kidney Int* **96**, 927–941 (2019).

796 63. Jo, S.-K., Cho, W. Y., Sung, S. A., Kim, H. K. & Won, N. H. MEK inhibitor, U0126, attenuates cisplatin-induced renal
797 injury by decreasing inflammation and apoptosis. *Kidney Int* **67**, 458–66 (2005).

798 64. Agoro, R., Montagna, A., Goetz, R., Aligbe, O., Singh, G., Coe, L. M., Mohammadi, M., Rivella, S. & Sitara, D.
799 Inhibition of fibroblast growth factor 23 (FGF23) signaling rescues renal anemia. *FASEB J* **32**, 3752–3764 (2018).

800 65. Courbon, G., Thomas, J. J., Martinez-Calle, M., Wang, X., Spindler, J., Von Drasek, J., Hunt-Tobey, B., Mehta, R.,
801 Isakova, T., Chang, W., Creemers, J. W. M., Ji, P., Martin, A. & David, V. Bone-derived C-terminal FGF23 cleaved
802 peptides increase iron availability in acute inflammation. *Blood* **142**, 106–118 (2023).

803

804

805

806

807

808 **FIGURE LEGENDS**

809 **Fig. 1. Elevated FGF23 levels in Hyp-Duk mice induces sustained-ERK signaling and**
810 **inflammatory, and immune gene signatures in the kidneys, which are mitigated by cFGF23 gene**
811 **therapy. A)** Graphical illustration showing the experimental design for the *in vivo* experiment. **B)** Mouse
812 iFGF23 levels in the serum of WT and Hyp-Duk mice (n=5, each group). **C)** Human cFGF23 levels in
813 the serum of WT, Hyp-Duk, and Hyp-Duk mice receiving AAV-FGF23 (cFGF23-Hyp-Duk); n=5, each
814 group; ND: not detected. **D)** Volcano plots illustrating DEGs identified by RNA-seq in the kidneys of WT,
815 Hyp-Duk, and cFGF23-Hyp-Duk mice. *Left panel*: DEGs compared between Hyp-Duk versus WT; *right*
816 *panel*: DEGs compared between cFGF23-Hyp-Duk versus Hyp-Duk. Note that numerous DEGs
817 identified in the kidneys of Hyp-Duk were significantly oppositely regulated in the kidneys of cFGF23-
818 Hyp-Duk mice. **E&F)** Gene expression levels of late- and early-ERK targets in the kidneys of WT, Hyp-
819 Duk, and cFGF23-Hyp-Duk mice. **G)** Fraction of transcriptome-inferred immune-like cells in kidneys of
820 WT, Hyp-Duk, and cFGF23-Hyp-Duk mice, as estimated by bulk RNA-seq deconvolution using
821 reference kidney single-cell transcriptomes. **H)** Heatmap of ImmPort DEGs in the kidneys of Hyp-Duk
822 rescued by AAV-cFGF23 treatment (block 1 and 2 represent downregulated and upregulated genes in
823 Hyp-Duk mice, respectively. **I)** Selected significantly upregulated GO pathways (biological processes)
824 in the kidneys of Hyp-Duk versus WT mice. Note that these pathways were either significantly or partially
825 rescued in the kidneys of cFGF23-Hyp-Duk mice. Dotted line indicates threshold for *padj<0.05*. The
826 pathway names in red indicate specific signal transduction pathways implicated in inflammatory and
827 immune gene signatures. **J&K)** Graphs illustrating representative genes implicated in GO pathways of
828 overall inflammatory and immune responses in the kidneys of WT, Hyp-Duk, and cFGF23-Hyp-Duk
829 mice. **L)** Urinary NGAL levels normalized to creatinine. n=5, each group. All values are expressed as
830 arithmetic means ± SE.

831

832 **Fig. 2. Effects of low versus high FGF23 concentrations (for 15 mins vs. 24 h) on ERK activation**
833 **and *EGR1* levels. A)** Original immunoblots of Klotho, pERK1/2 and tERK1/2 upon treatment with 0.5
834 nM and 10 nM FGF23 in HEK^{Kl} and HEK^{Wt} cells for 15 min and 24 hrs. **B)** Original immunoblots of
835 pERK1/2 and ERK in HEK^{Kl} cells upon treating with increasing concentrations of FGF23 for 24 hours.
836 **C&D)** Fold change *EGR1* mRNA levels, normalized to *GAPDH* upon treating 0.5 nM and 10 nM FGF23
837 in HEK^{Kl}/HEK^{Wt} cells over 24 hours, respectively (n=3). *p* values in red and teal indicate comparisons
838 between FGF23 vs control treatment in HEK^{Kl} and HEK^{Wt} cells, respectively. ns=p>0.05. **E)** *EGR1*
839 mRNA, normalized to *GAPDH,* upon treating with 0.5 nM and 10 nM FGF23 for 24 hours in HEK^{Kl} cells.
840 n=3, each group. All the values are expressed as arithmetic means ± SE.

841

842 **Fig. 3. Identification of temporal ERK signaling by physiological versus pathological FGF23**
843 **concentrations. A)** Graphic illustration showing the experimental design for RNA-seq. **B&C)** Volcano
844 plots illustrating all the genes identified by RNA-seq upon physiological and FGF23 pathological in
845 HEK^{Wt}/HEK^{Kl} cells, respectively. The upregulated and downregulated genes (abs(log2FC)>1) are
846 shown in red and blue, respectively. **D)** ERK targets that are statistically significantly upregulated by
847 physiological FGF23 compared to pathological FGF23 in HEK^{Kl} cells. The gene expression is compared

848 to the corresponding control. **E)** ERK targets that are either statistically significantly unchanged or
849 upregulated by pathological FGF23 compared to physiological FGF23 in HEK^{KI} cells. The gene
850 expression is compared to the corresponding control. **F)** Venn diagram showing DEGs compared
851 between physiological FGF23 and pathological FGF23 in HEK^{KI} cells (padj<0.05; (abs(log2FC)>1). **G)**
852 Selected upregulated GO pathways in biological processes enriched upon pathological FGF23 in HEK^{KI}
853 cells (padj<0.05; log2Fc>1). The red arrows indicate pathways implicated in inflammatory and immune
854 gene signatures. **H)** Heatmap highlighting DEGs by pathological FGF23 in HEK^{KI} cells that were present
855 in the ImmPort database. Block 1 represents DEGs only affected by pathological FGF23, while block 2
856 represents DEGs affected by both pathological and physiological FGF23. Exemplary
857 immune/inflammatory genes reported in literature are shown in red. **I)** Representative transcripts
858 implicated in inflammatory and immune gene signature and upregulated only by pathological FGF23 in
859 HEK^{KI} cells (red bars). Note that these genes are unchanged by similar treatment in HEK^{Wt} cells (grey
860 bars). (n=3), ns=padj>0.05. All the values are expressed as arithmetic means ± SE.
861
862 **Fig. 4. HEK^{KI} cells model renal transcriptional programs downstream of FGF23-Klotho signaling.**
863 **(A)** Heatmaps showing relative expression of late ERK-responsive genes in HEK^{KI} cells treated with
864 pathological FGF23 compared with PBS control (n = 3 per group; P < 0.05) and in kidneys from Hyp-
865 Duk (Hyp) versus wild-type (WT) mice (n = 5 per group; P < 0.05). **(B)** Heatmaps showing relative
866 expression of inflammatory and immune-related genes in HEK^{KI} cells (Patho. FGF23 vs. PBS; n = 3 per
867 group; P < 0.05) and Hyp-Duk versus WT kidneys (n = 5 per group; P < 0.05).
868
869 **Fig. 5. Pathological FGF23-mediated ERK signaling, inflammatory and immune gene signatures**
870 **are inhibited by FGFR and MEK blockers. A)** *EGR1* and *ETV4* mRNA, normalized to *GAPDH*, upon
871 treating HEK^{KI} cells with 10 nM FGF23 for 24 hours with or without FGFR inhibitor (PD173074) or MEK
872 inhibitor (U0126) (n=3). **B)** mRNA levels of *TNFRSF9*, *TNFRSF12A*, *GDF15*, *ANXA1*, and *TGFB1*
873 normalized to *GAPDH*, upon treating HEK^{KI} cells with pathological FGF23 (10 nM FGF23 for 24 hours)
874 with or without FGFR inhibitor or MEK inhibitor (n=3). All values are expressed as arithmetic means ±
875 SE.
876
877 **Fig. 6. Pathological FGF23-mediated ERK signaling, inflammatory and immune gene signature**
878 **is mitigated by cFGF23. A)** Graphical illustration showing mechanisms of action of the cFGF23
879 peptide. *Left panel:* Intact full-length iFGF23 harbors its C-terminus cFGF23 and N-terminus nFGF23.
880 Within iFGF23, cFGF23 and nFGF23 bind with co-receptors Klotho and FGFR, respectively, and
881 activate ERK signaling. *Right panel:* High concentration of the cFGF23 peptide competes with iFGF23
882 for binding with Klotho and thus mitigates ERK signaling. **B)** *EGR1* and *ETV4* mRNA, normalized to
883 *GAPDH*, upon treating HEK^{KI} cells with pathological FGF23 (10 nM FGF23 for 24 hours) with or without
884 increasing concentrations of cFGF23 (n=3). **C)** mRNA levels of *TNFRSF9*, *TNFRSF12A*, *GDF15*,
885 *ANXA1*, and *TGFB1* normalized to *GAPDH*, upon treating HEK^{KI} cells with pathological FGF23 with or
886 without increasing concentrations of cFGF23 (n=3). All values are expressed as arithmetic means ± SE.
887

888 **Fig. 7. Proposed model: Left Panel:** In diseases where FGF23 is chronically elevated, the FGF23-
889 FGFR-Klotho-HS signaling complex induces sustained-ERK activation in the cytoplasm. ERK is
890 continuously and irreversibly translocated to the nucleus, where it upregulates late-ERK targets along
891 with inflammation and immune gene signatures. It is currently unclear whether late-ERK targets directly
892 activate inflammation and immune gene signatures. The cFGF23 peptide blocks FGF23-Klotho binding,
893 thereby inhibiting downstream ERK signaling as well as inflammation and immune gene signatures.
894 **Right Panel**: Physiological rise in FGF23 rapidly and reversibly activate ERK in the cytoplasm via
895 FGF23-FGFR-Klotho-HS signaling complex. In this case, ERK transiently translocates to the nucleus
896 and upregulates early-ERK targets and is less likely to regulate gene signatures implicated in
897 inflammation and immune responses.

Fig. 1

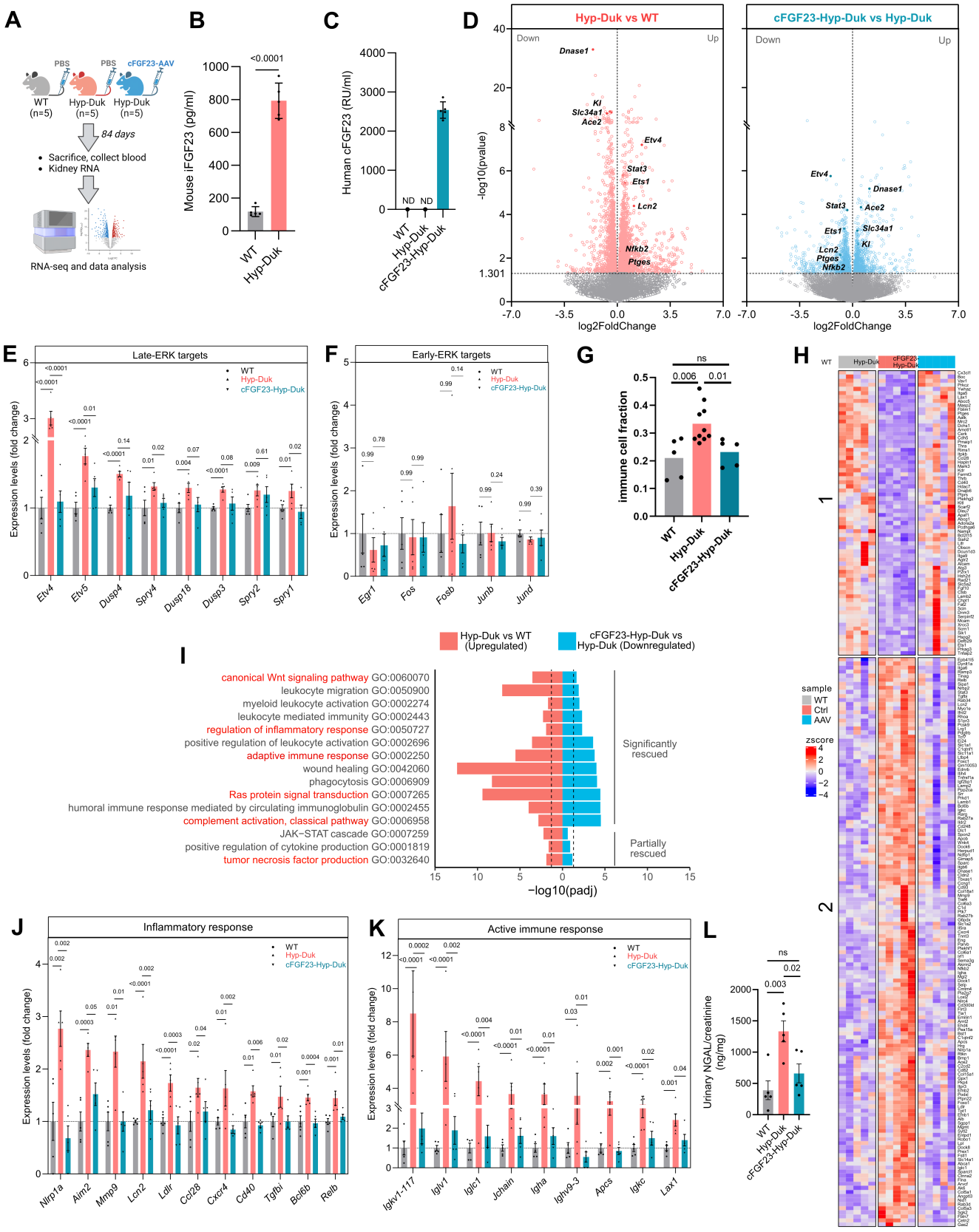
A
PBS
PBS
cFGF23-AAV
WT (n=5)
Hyp-Duk (n=5)
Hyp-Duk (n=5)
84 days
Sacrifice, collect blood
Kidney RNA
RNA-seq and data analysis
B
Mouse iFGF23 (pg/ml)
<0.0001
WT
Hyp-Duk
C
Human cFGF23 (RU/ml)
ND
ND
WT
Hyp-Duk
cFGF23-Hyp-Duk
D
Hyp-Duk vs WT
cFGF23-Hyp-Duk vs Hyp-Duk
Down
Up
-log10(pvalue)
log2FoldChange
Dnase1
Kl
Slc34a1
Ace2
Etv4
Stat3
Ets1
Lcn2
Nfkb2
Ptges
E
Late-ERK targets
Expression levels (fold change)
WT
Hyp-Duk
cFGF23-Hyp-Duk
Etv4
Etv5
Dusp4
Spry4
Dusp18
Dusp3
Spry2
Spry1
F
Early-ERK targets
Egr1
Fos
Fosb
Junb
Jund
G
immune cell fraction
ns
0.006
0.01
WT
Hyp-Duk
cFGF23-Hyp-Duk
H
WT
Hyp-Duk
cFGF23-Hyp-Duk
sample
WT
Ctrl
AAV
zscore
I
Hyp-Duk vs WT (Upregulated)
cFGF23-Hyp-Duk vs Hyp-Duk (Downregulated)
canonical Wnt signaling pathway GO:0060070
leukocyte migration GO:0050900
myeloid leukocyte activation GO:0002274
leukocyte mediated immunity GO:0002443
regulation of inflammatory response GO:0050727
positive regulation of leukocyte activation GO:0002696
adaptive immune response GO:0002250
wound healing GO:0042060
phagocytosis GO:0006909
Ras protein signal transduction GO:0007265
humoral immune response mediated by circulating immunoglobulin GO:0002455
complement activation, classical pathway GO:0006958
JAK−STAT cascade GO:0007259
positive regulation of cytokine production GO:0001819
tumor necrosis factor production GO:0032640
Significantly rescued
Partially rescued
−log10(padj)
J
Inflammatory response
Expression levels (fold change)
WT
Hyp-Duk
cFGF23-Hyp-Duk
Nlrp1a
Aim2
Mmp9
Lcn2
Ldlr
Ccl28
Cxcr4
Cd40
Tgfbi
Bcl6b
Relb
K
Active immune response
Expression levels (fold change)
WT
Hyp-Duk
cFGF23-Hyp-Duk
Igkv1-117
Iglv1
Iglc1
Jchain
Igha
Ighv9-3
Apcs
Igkc
Lax1
L
Urinary NGAL/creatinine (ng/mg)
ns
0.02
0.003
WT
Hyp-Duk
cFGF23-Hyp-Duk

Fig. 2

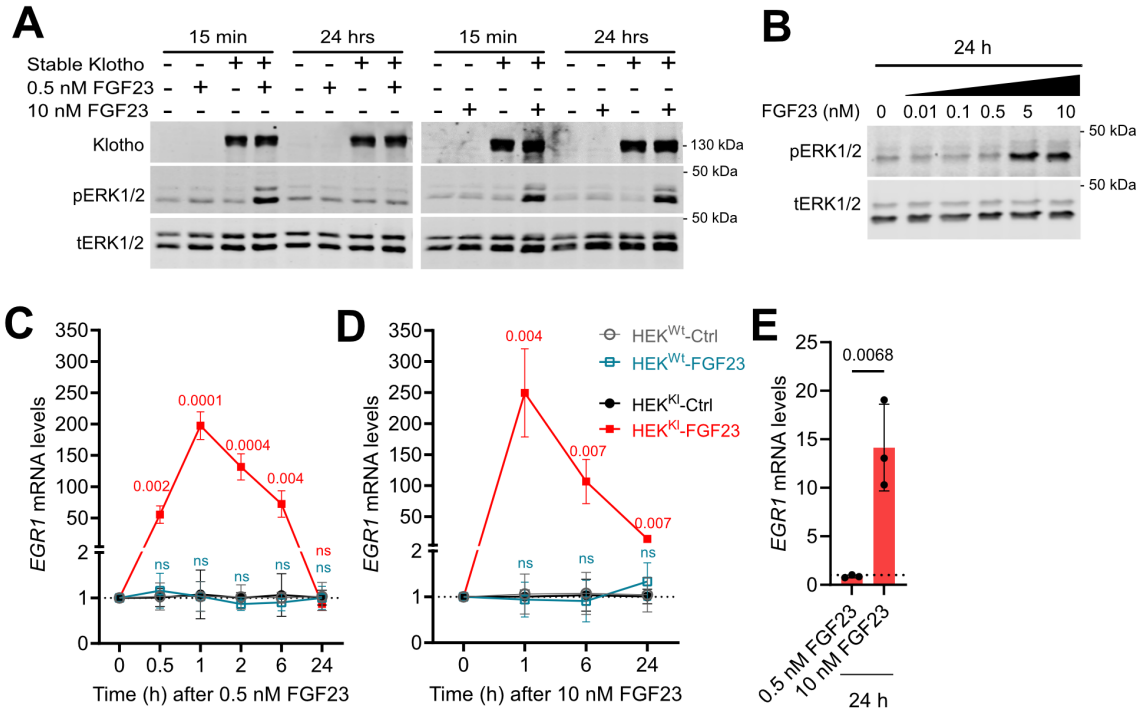
A
15 min
24 hrs
15 min
24 hrs
Stable Klotho
0.5 nM FGF23
10 nM FGF23
Klotho
pERK1/2
tERK1/2
130 kDa
50 kDa
50 kDa
B
24 h
FGF23 (nM) 0 0.01 0.1 0.5 5 10
pERK1/2
tERK1/2
50 kDa
50 kDa
C
EGR1 mRNA levels
0.0001
0.0004
0.002
0.004
ns
Time (h) after 0.5 nM FGF23
D
HEKWt-Ctrl
HEKWt-FGF23
HEKKI-Ctrl
HEKKI-FGF23
0.004
0.007
0.007
Time (h) after 10 nM FGF23
E
0.0068
0.5 nM FGF23
10 nM FGF23
24 h

Fig. 3

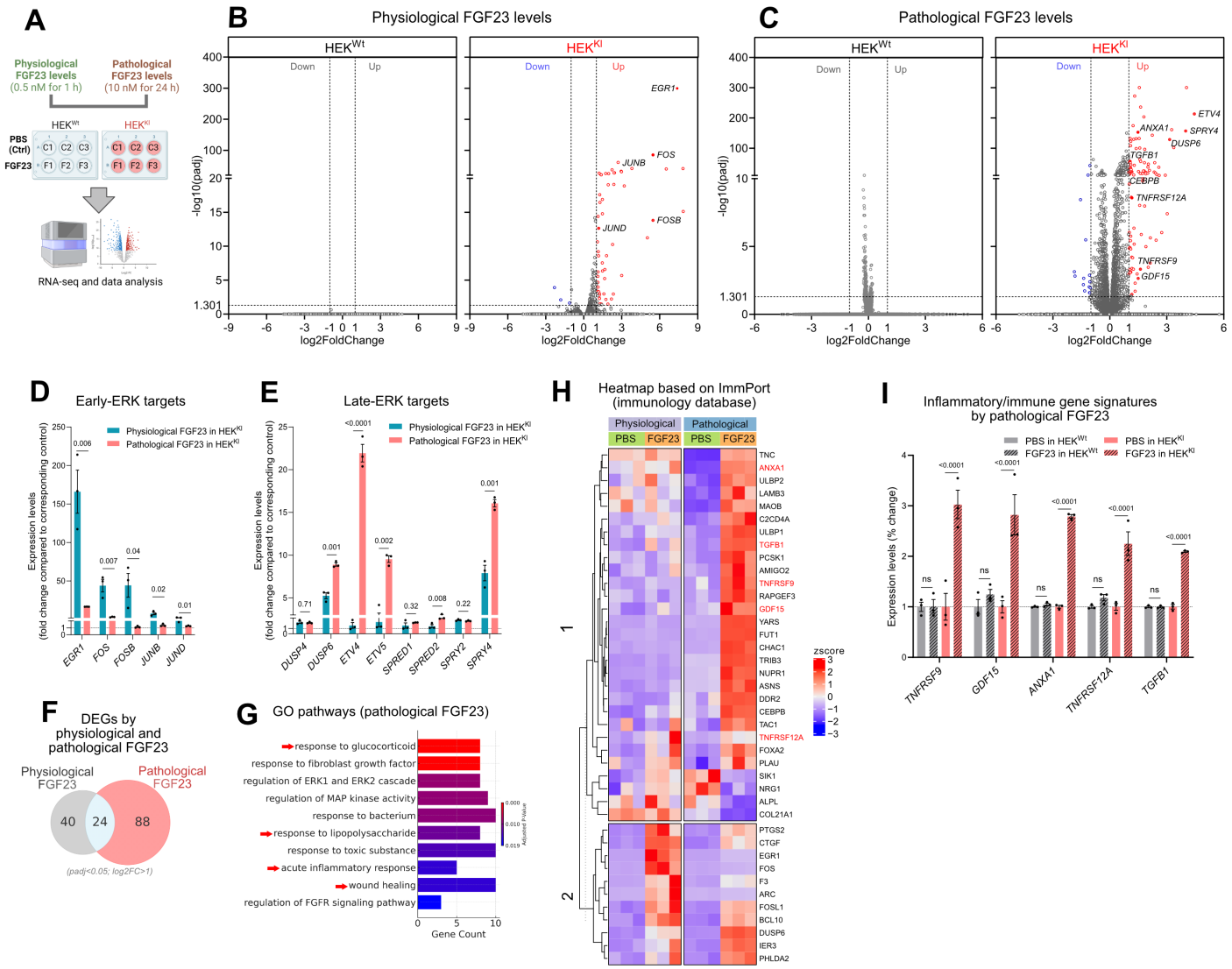
A
Physiological FGF23 levels (0.5 nM for 1 h)
Pathological FGF23 levels (10 nM for 24 h)
HEK^Wt
HEK^KI
PBS (Ctrl)
FGF23
RNA-seq and data analysis
B
Physiological FGF23 levels
HEK^Wt
HEK^KI
Down
Up
EGR1
FOS
JUNB
FOSB
JUND
-log10(padj)
log2FoldChange
C
Pathological FGF23 levels
ETV4
ANXA1
SPRY4
DUSP6
TGFB1
CEBPB
TNFRSF12A
TNFRSF9
GDF15
D
Early-ERK targets
Physiological FGF23 in HEK^KI
Pathological FGF23 in HEK^KI
Expression levels (fold change compared to corresponding control)
EGR1
FOS
FOSB
JUNB
JUND
E
Late-ERK targets
DUSP4
DUSP6
ETV4
ETV5
SPRED1
SPRED2
SPRY2
SPRY4
F
DEGs by physiological and pathological FGF23
Physiological FGF23
Pathological FGF23
40
24
88
(padj<0.05; log2FC>1)
G
GO pathways (pathological FGF23)
response to glucocorticoid
response to fibroblast growth factor
regulation of ERK1 and ERK2 cascade
regulation of MAP kinase activity
response to bacterium
response to lipopolysaccharide
response to toxic substance
acute inflammatory response
wound healing
regulation of FGFR signaling pathway
Gene Count
Adjusted P-Value
H
Heatmap based on ImmPort (immunology database)
Physiological
Pathological
PBS
FGF23
zscore
TNC
ANXA1
ULBP2
LAMB3
MAOB
C2CD4A
ULBP1
TGFB1
PCSK1
AMIGO2
TNFRSF9
RAPGEF3
GDF15
YARS
FUT1
CHAC1
TRIB3
NUPR1
ASNS
DDR2
CEBPB
TAC1
TNFRSF12A
FOXA2
PLAU
SIK1
NRG1
ALPL
COL21A1
PTGS2
CTGF
EGR1
FOS
F3
ARC
FOSL1
BCL10
DUSP6
IER3
PHLDA2
I
Inflammatory/immune gene signatures by pathological FGF23
PBS in HEK^Wt
FGF23 in HEK^Wt
PBS in HEK^KI
FGF23 in HEK^KI
Expression levels (% change)
TNFRSF9
GDF15
ANXA1
TNFRSF12A
TGFB1

Fig. 4

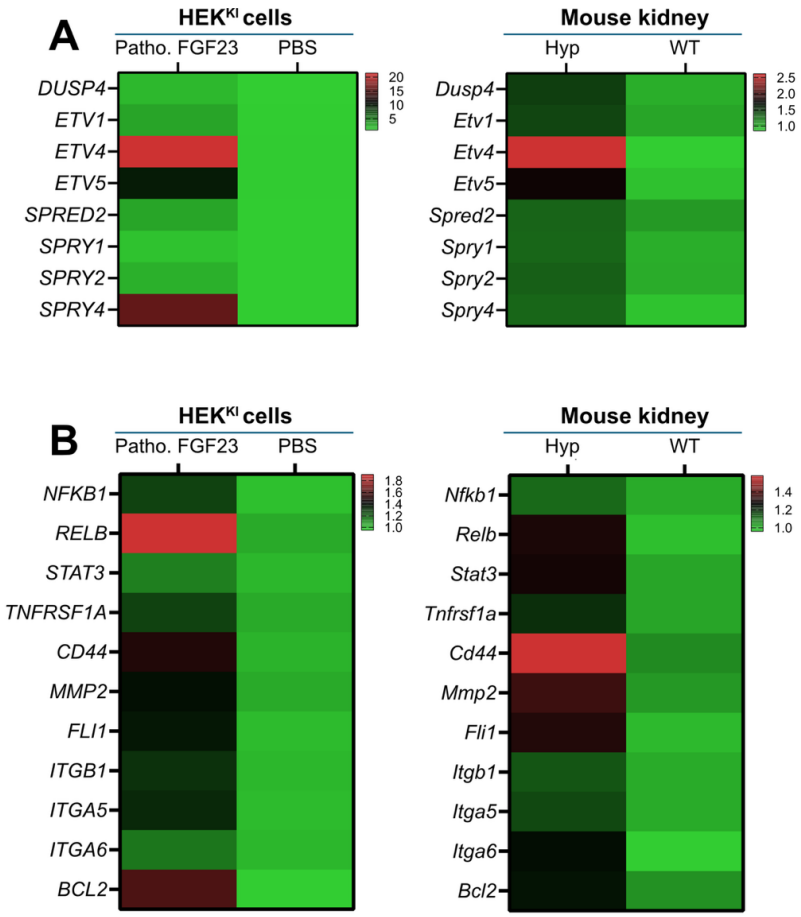
A
HEK^KI cells
Patho. FGF23
PBS
DUSP4
ETV1
ETV4
ETV5
SPRED2
SPRY1
SPRY2
SPRY4
20
15
10
5
Mouse kidney
Hyp
WT
Dusp4
Etv1
Etv4
Etv5
Spred2
Spry1
Spry2
Spry4
2.5
2.0
1.5
1.0
B
HEK^KI cells
Patho. FGF23
PBS
NFKB1
RELB
STAT3
TNFRSF1A
CD44
MMP2
FLI1
ITGB1
ITGA5
ITGA6
BCL2
1.8
1.6
1.4
1.2
1.0
Mouse kidney
Hyp
WT
Nfkb1
Relb
Stat3
Tnfrsf1a
Cd44
Mmp2
Fli1
Itgb1
Itga5
Itga6
Bcl2
1.4
1.2
1.0

Fig. 5

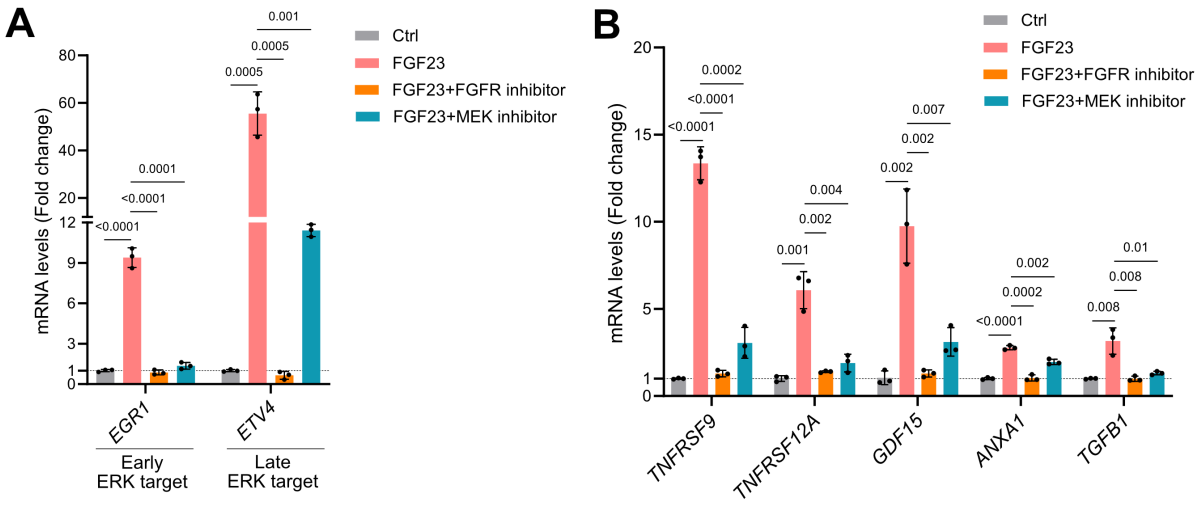
A
mRNA levels (Fold change)
80
60
40
20
12
9
6
3
1
0
<0.0001
<0.0001
0.0001
0.0005
0.0005
0.001
EGR1
ETV4
Early ERK target
Late ERK target
Ctrl
FGF23
FGF23+FGFR inhibitor
FGF23+MEK inhibitor
B
mRNA levels (Fold change)
20
15
10
5
1
0
<0.0001
<0.0001
0.0002
0.001
0.002
0.004
0.002
0.002
0.007
<0.0001
0.0002
0.002
0.008
0.008
0.01
TNFRSF9
TNFRSF12A
GDF15
ANXA1
TGFB1
Ctrl
FGF23
FGF23+FGFR inhibitor
FGF23+MEK inhibitor

Fig. 6

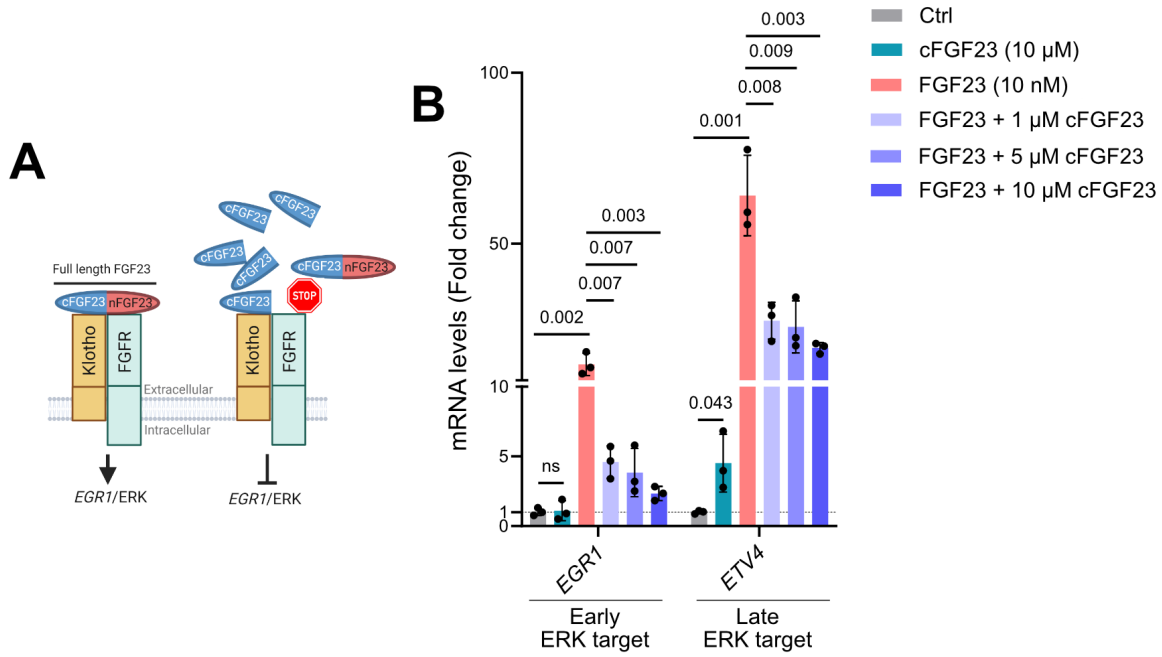
A
Full length FGF23
cFGF23
nFGF23
Klotho
FGFR
Extracellular
Intracellular
EGR1/ERK
STOP
B
mRNA levels (Fold change)
100
50
10
5
1
0
ns
0.002
0.007
0.007
0.003
0.043
0.001
0.008
0.009
0.003
EGR1
ETV4
Early ERK target
Late ERK target
Ctrl
cFGF23 (10 μM)
FGF23 (10 nM)
FGF23 + 1 μM cFGF23
FGF23 + 5 μM cFGF23
FGF23 + 10 μM cFGF23

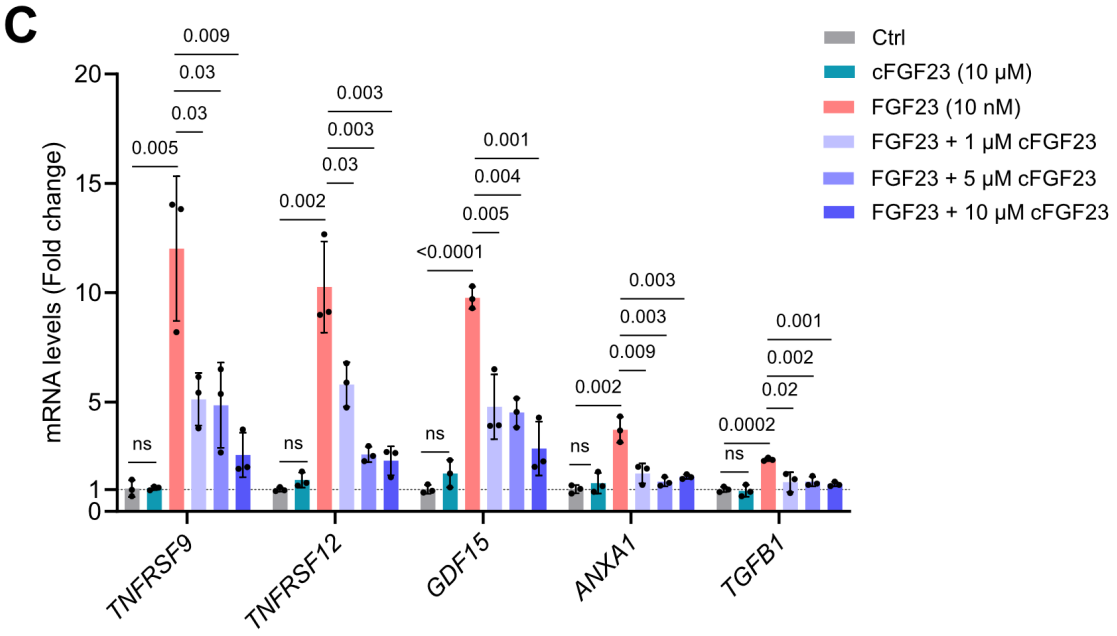
C
mRNA levels (Fold change)
20
15
10
5
1
0
ns
0.005
0.03
0.03
0.009
ns
0.002
0.03
0.003
0.003
ns
<0.0001
0.005
0.004
0.001
ns
0.002
0.009
0.003
0.003
0.0002
ns
0.02
0.002
0.001
TNFRSF9
TNFRSF12
GDF15
ANXA1
TGFB1
Ctrl
cFGF23 (10 μM)
FGF23 (10 nM)
FGF23 + 1 μM cFGF23
FGF23 + 5 μM cFGF23
FGF23 + 10 μM cFGF23

Fig. 7

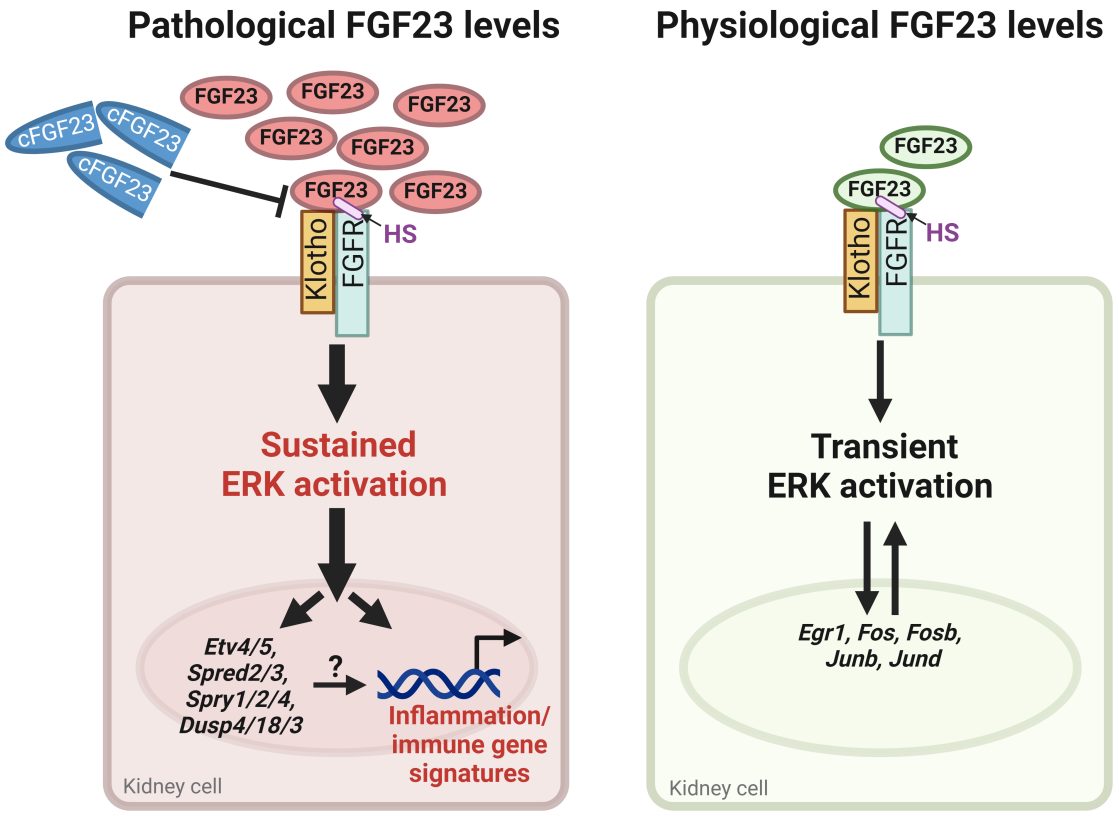
Pathological FGF23 levels
Physiological FGF23 levels
FGF23
cFGF23
Klotho
FGFR
HS
Sustained
ERK activation
Etv4/5,
Spred2/3,
Spry1/2/4,
Dusp4/18/3
?
Inflammation/
immune gene
signatures
Kidney cell
Transient
ERK activation
Egr1, Fos, Fosb,
Junb, Jund
Kidney cell

898